ENDOCRINOLOGY AND METABOLISM.

RESEARCH ARTICLE

Chronic inorganic nitrate supplementation does not improve metabolic health and worsens disease progression in mice with diet-induced obesity

© Alice P. Sowton,¹ Lorenz M. W. Holzner,¹ Fynn N. Krause,² © Ruby Baxter,¹ Gabriele Mocciaro,² Dominika K. Krzyzanska,¹ © Magdalena Minnion,³ Katie A. O'Brien,¹ Matthew C. Harrop,¹ Paula M. Darwin,¹ Benjamin D. Thackray,¹ © Michele Vacca,^{2,4} © Martin Feelisch,³ Julian L. Griffin,^{2,5} and © Andrew J. Murray¹

¹Department of Physiology, Development and Neuroscience, University of Cambridge, Cambridge, United Kingdom; ²Department of Biochemistry and Systems Biology Centre, University of Cambridge, Cambridge, United Kingdom; ³Clinical & Experimental Sciences, Faculty of Medicine, University of Southampton, Southampton, United Kingdom; ⁴Wellcome Trust-MRC Institute of Metabolic Science Metabolic Research Laboratories, Addenbrooke's Hospital, Cambridge, United Kingdom; and ⁵The Rowett Institute, University of Aberdeen, Aberdeen, United Kingdom

Abstract

Inorganic nitrate (NO_3^-) has been proposed to be of therapeutic use as a dietary supplement in obesity and related conditions including the metabolic syndrome (MetS), type II diabetes, and metabolic dysfunction-associated steatotic liver disease (MASLD). Administration of NO_3^- to endothelial nitric oxide synthase-deficient mice reversed aspects of MetS; however, the impact of NO_3^- supplementation in diet-induced obesity is not well understood. Here we investigated the whole body metabolic phenotype and cardiac and hepatic metabolism in mice fed a high-fat, high-sucrose (HFHS) diet for up to 12 mo of age, supplemented with 1 mM $NaNO_3$ (or NaCl) in their drinking water. HFHS feeding was associated with a progressive obesogenic and diabetogenic phenotype, which was not ameliorated by NO_3^- . Furthermore, HFHS-fed mice supplemented with NO_3^- showed elevated levels of cardiac fibrosis and accelerated progression of MASLD including development of hepatocellular carcinoma in comparison with NaCl-supplemented mice. NO_3^- did not enhance mitochondrial β -oxidation capacity in any tissue assayed and did not suppress hepatic lipid accumulation, suggesting it does not prevent lipotoxicity. We conclude that NO_3^- is ineffective in preventing the metabolic consequences of an obesogenic diet and may instead be detrimental to metabolic health against the background of HFHS feeding. This is the first report of an unfavorable effect of long-term nitrate supplementation in the context of the metabolic challenges of overfeeding, warranting urgent further investigation into the mechanism of this interaction.

NEW & NOTEWORTHY Inorganic nitrate has been suggested to be of therapeutic benefit in obesity-related conditions, as it increases nitric oxide bioavailability, enhances mitochondrial β -oxidation, and reverses metabolic syndrome in $eNOS^{-/-}$ mice. However, we here show that over 12 months nitrate was ineffective in preventing metabolic consequences in high fat, high sucrose-fed mice and worsened aspects of metabolic health, impairing cholesterol handling, increasing cardiac fibrosis, and exacerbating steatotic liver disease progression, with acceleration to hepatocellular carcinoma.

inorganic nitrate; metabolic dysfunction-associated steatotic liver disease; metabolism; mitochondria; obesity

INTRODUCTION

The obesity epidemic remains a global health concern, and its prevalence continues to increase worldwide (1). Obesity is associated with high morbidity and mortality (2), largely due to the elevated risk of comorbidities such as type II diabetes mellitus (T2DM), cardiovascular disease (CVD), and metabolic dysfunction-associated steatotic liver disease (MASLD), a condition previously known as nonalcoholic fatty liver disease (NAFLD) (3–7).

Obesity and diabetes are associated with hypertension (8), which is in turn associated with endothelial dysfunction and reduced nitric oxide (NO) bioavailability. Mice

lacking endothelial nitric oxide synthase ($eNOS^{-/-}$ mice) are hypertensive (9) but also develop symptoms of the metabolic syndrome (MetS) including glucose intolerance and dyslipidemia, alongside hyperleptinemia (10, 11) and defective mitochondrial β -oxidation and biogenesis (12, 13). In humans, eNOS polymorphisms have been associated with T2DM and MetS (14, 15), whereas patients with T2DM generate less NO from L-arginine than healthy control subjects (16). NO production and metabolism, particularly decreased NO bioavailability, are therefore considered central to the etiology of MetS/T2DM.

Canonical formation of NO occurs via oxidation of a guanidino nitrogen of L-arginine by one of three isoforms of





NOS. However, it is now recognized that NO can also be produced via reduction of endogenously produced or dietary inorganic nitrate (NO₃⁻) (17). In the circulation, NO generated by the vascular endothelium is oxidized to nitrite (NO₂⁻) and nitrate. The latter is taken up from the blood and secreted into saliva, where it is reduced to nitrite by commensal bacterial flora of the mouth (18). Upon swallowing of saliva, NO₂⁻ is rapidly protonated in the stomach, forming nitrous acid (HNO₂), which spontaneously decomposes to form NO (19, 20). Remaining nitrate or nitrite can be absorbed in the intestine, where nitrite can be reduced to NO by enzymes including xanthine oxidoreductase, deoxyhemoglobin, and myoglobin (21-23). Circulating NO₃⁻ is eventually excreted by the kidneys, although \sim 25% is actively taken up by the salivary glands, allowing it to be concentrated in saliva and recirculated (17, 20). Thus, inorganic nitrate, once considered an end product of NO metabolism (24) and, along with nitrite, a potentially toxic residue of food preservation (25), is now recognized as a potentially important source of NO under hypoxic and acidotic conditions (20, 26) and a route to modulate NO bioavailability via dietary manipulation (20). Both nitrite and nitrate were used medicinally long before any of these mechanisms had been discovered (27).

Dietary supplementation with inorganic nitrate for 8-10 wk reverses features of MetS in eNOS^{-/-} mice, improving glucose handling, hypertension, and dyslipidemia (28). It is not established whether reduced NO bioavailability is a universal feature of MetS and/or T2DM; however, nitrite improved glycemia in db/db mice (1-mo treatment) (29) and ob^{lep} mice (1-wk treatment) (30), whereas nitrate improved insulin sensitivity in high fructose-fed rats over 10 wk (31), high-fat diet low-dose streptozotocin T2DM rats over 2 mo (32), and high fat, high fructose-fed mice over 1 mo (33). At a tissue level, dietary nitrate increased mitochondrial β-oxidation in the heart and skeletal muscle of rats and mice (34–36) and was associated with increased voluntary wheel running in mice (37). Dietary inorganic nitrate enhanced white adipose tissue browning in rats (38) and increased mitochondrial oxygen consumption (39) and glucose oxidation (40) in white adipocytes. In liver, NO (generated by eNOS) inhibits activation of proinflammatory Kupffer cells, a response characteristic of MASLD pathogenesis (41). Although longterm (17 mo) nitrate supplementation did not result in adverse health effects in healthy mice and was associated with improved insulin sensitivity (42), the long-term implications of nitrate supplementation in obese animals remain unknown. This could be of particular importance in light of the effects of overfeeding with lipids and carbohydrates on mitochondrial function and reactive oxygen species (ROS) production against the complex interaction with tissue and whole body redox regulation vis-à-vis aging-related alterations in metabolic regulation by liver and skeletal muscle.

We therefore sought to investigate whether dietary supplementation with a moderate dose of inorganic nitrate (similar to that achievable with a human diet rich in leafy vegetables) ameliorates the progression of metabolic comorbidities associated with diet-induced obesity in mice. We hypothesized that inorganic nitrate would delay the development of metabolic and mitochondrial dysregulation in high fat, high sucrose-fed mice via enhanced NO bioavailability and modulation of tissue mitochondrial function.

MATERIALS AND METHODS

Chemicals

Unless otherwise stated, all reagents were purchased from Sigma-Aldrich (Merck Life Science UK, Gillingham, UK).

Ethical Approval

All studies were carried out in accordance with United Kingdom Home Office legislation under the Animals in Scientific Procedures (1986) Act and received prior approval from the University of Cambridge Animal Welfare and Ethical Review Board. All procedures were carried out by a personal license holder in accordance with these regulations.

Study Design

Male C57Bl/6J mice (n = 95; RRID: MGI:3028467) were purchased from a commercial breeder (Charles River Laboratories, Margate, UK) at 3 wk of age. Unless otherwise stated, all mice were group-housed in conventional cages under controlled environmental conditions (21°C, 54% humidity, 12-h photoperiod) and were allowed ad libitum access to food and water for the duration of the study.

In the first week of vivarium acclimatization, mice received a standard laboratory rodent chow diet [RM3(E); Special Diet Services, Essex, UK; 3.6 kcal·g⁻¹, 39.7% carbohydrate, 22.4% crude protein, 4.3% crude fat; referred to here as "chow" and distilled water ad libitum. From 4 wk of age, mice were randomized into four experimental groups (n = 23-24/group): two groups continued to receive chow, and the others received a high-saturated fat, highsucrose (HFHS) diet (TD.88137; Envigo Teklad Diets, Madison, WI; $4.5 \text{ kcal} \cdot \text{g}^{-1}$, 48.5% carbohydrate, 17.3% crude protein, 21.2% crude fat). Within each diet group, one experimental group received drinking water supplemented with 1 mM sodium nitrate (NaNO₃; TraceSELECT, no. 71752, Fluka; Honeywell Specialty Chemicals, Seelze, Germany) and the other received water supplemented with 1 mM sodium chloride (NaCl; TraceSELECT, no. 38979, Fluka) to control for sodium intake. Mice were maintained on their respective diets/treatments until they reached 4, 8, or 12 mo of age (n = 7 or 8/group; Fig. 1A). Body mass, food, and water intake were measured weekly.

Five (±2) days before the end of the treatment period, mice were fasted overnight before blood was sampled from the lateral tail vein for determination of fasting blood glucose (Accu-Chek Compact glucometer; Roche) and plasma separated (4,000 g, 10 min, 4°C, K₃EDTA anticoagulant) and snap frozen for clinical chemistry analyses.

At 4, 8, or 12 mo of age (±2 days) mice were terminally anesthetized via an intraperitoneal injection of sodium pentobarbital (500 ${\rm mg\cdot kg^{-1}}$, Euthatal Solution; Merial Animal Health Ltd., Bracknell, UK). A terminal (fed state) blood sample was collected via cardiac puncture and the plasma separated and snap frozen for later analyses. The heart was rapidly excised, atria and extraneous tissue removed, and the heart weighed before the apex was removed and placed into ice-cold biopsy-preservation medium [BIOPS (in mM): 2.77 CaK₂EGTA, 7.23 K₂EGTA, 6.56 MgCl₂, 50 MES, 5.77 ATP, 15 phosphocreatine (PCr), 20 imidazole, 20 taurine, and 0.5

dithiothreitol, pH 7.1]. A transverse midsection 1-2 mm above the apex was carefully sectioned and placed into icecold paraformaldehyde (PFA) (4% in phosphate-buffered saline, no. J61899; Alfa-Asaer, Heysham, UK) for subsequent histological analysis, before the remaining left ventricle was separated and snap frozen. The liver was removed from the abdominal cavity and the left lateral lobe (LLL) quickly divided into three equal sections; one section was placed into ice-cold BIOPS, one section placed in neutral buffered formalin (no. 11699455; VWR International, Lutterworth, UK), and the remaining third snap frozen for molecular analyses. The right lateral lobe was fixed in isopentane precooled in dry ice.

After removal of the heart and liver, the carcass was weighed, nose-to-anus length measured, and body composition determined by dual-energy X-ray absorptiometry (DEXA) (Lunar PIXImus II; GE Medical Systems Ltd.). Body composition parameters were calculated with PIXImus software (Lunar Corporation, Madison, WI) after exclusion of the skull, per the manufacturer's instructions. After the DEXA scan, the right soleus and gastrocnemius muscles were dissected and placed into ice-cold BIOPS. The left tibia was also dissected and boiled for >5 h to remove all soft tissue, then precisely measured from the tibial plateau to the tip of the medial malleolus.

Metabolic Cages

For the 12-mo cohort, mice underwent a 48-h metabolic cage (Promethion; Sable Systems, Germany) protocol at 10 mo (±6 days) of age. Mice were acclimatized to indirect calorimetry cages (Promethion; Sable Systems, Germany) for 24 h before data collection. Cages were housed in a thermostatic, light-cycling cabinet (CAB-16; Sable Systems) to maintain constant temperature, humidity, and photoperiod equivalent to home cages throughout the experimental period.

Each mouse had ad libitum access to food and water of its relevant dietary intervention throughout its time in the metabolic cages, which was continuously measured via MM-2 load cells (Promethion; Sable Systems) precalibrated to known masses. Indirect calorimetry was achieved through a pull-mode air flow generator (Promethion Core CGF; Sable Systems), calibrated to wet and dry air and 0 to 5,000 ppm carbon dioxide. Air was pulled through each metabolic cage at 2 L·min⁻¹, with subsamples analyzed for oxygen, carbon dioxide, and water vapor, allowing measurement of oxygen consumption ($\dot{V}o_2$) and carbon dioxide production ($\dot{V}co_2$) from each mouse.

Data were collected with a 1-Hz sampling rate and acquired and coordinated by the IM3 Interface Module (v20.0.6; Sable Systems), with real-time measurement of respiratory exchange ratio (RER) and calculation of energy expenditure (EE, via the Weir equation) (45). Data were processed with ExpeData (v1.9.27; Sable Systems) with Macro Interpreter (v2.32; Sable Systems) to process raw data into 5-min bins. Metabolic cage data were corrected to body mass, lean mass, or fat mass covariates, as appropriate (46), determined by time-domain nuclear magnetic resonance (TD-NMR) (LF50H Minispec; Bruker, Coventry, UK). TD-NMR data were acquired with minispec software (v3.0, connected to OPUS v7.0; both Bruker). Data were analyzed with the CalR framework (RRID: SCR_015859) (47), adapted for a 2×2 factorial design, in R (48).

Blood Analyses

Insulin, free fatty acids (FFA), triacylglycerols (TAG), total cholesterol, and HDL cholesterol were measured in fasted blood samples by the Core Biochemical Assay Laboratory (Cambridge University Hospitals, NHS Foundation Trust, Cambridge, UK). LDL cholesterol was calculated with the Friedewald equation (49). Fasted glucose and insulin measurements were used to calculate the homeostatic model assessment (43) as a measurement of insulin resistance (HOMA-IR) adapted for murine models, as previously described (50).

Plasma nitrate and nitrite concentrations were determined in the fed state with a dedicated high-performance liquid chromatography analysis system (Eicom ENO-30, coupled to an AS-700 INSIGHT autosampler; Amuza Inc.) after methanol deproteinization as previously described (51). Plasma concentrations of the liver enzymes alanine transaminase (ALT) and aspartate transaminase (AST) were quantified via commercial ELISAs (no. ab28282 and no. ab263882; Abcam, Cambridge, UK). The antioxidant capacity of plasma was determined via the ferric reducing ability of plasma (FRAP) assay, as previously described (52). Lipid peroxidation was used as a marker of oxidative stress and quantified in plasma by measurement of thiobarbituric acid reactive substances (TBARS), as previously described (52).

Intestinal Morphology

For investigation of intestinal morphology, an additional cohort of male C57Bl/6J mice (aged 8 wk, n = 7) was purchased from the same commercial breeder and randomized to receive either standard laboratory chow [RM3(E)] or HFHS diet (TD.88137). After 14 wk, mice were terminally anesthetized and the gastrointestinal tract dissected from the pyloric sphincter to the rectum. After the cecum was removed, the intestinal tract was cut into four sections (colon, plus proximal, mid, and distal small intestine approximately equivalent to the duodenum, jejunum, and ileum) and prepared for histological processing, as previously described (53).

Hepatic Lipid Content

Hepatic lipid content was quantified with an optimized Folch extraction protocol for quantification of liver fat (54).

High-Resolution Respirometry

High-resolution respirometry was performed with an Oxygraph-2k (Oroboros Instruments, Innsbruck, Austria) on saponin-permeabilized muscle fiber bundles from the cardiac apex, soleus and gastrocnemius muscles, and liver left lateral lobe (LLL) homogenate, prepared as previously described (55, 56). A substrate-uncoupler-inhibitor titration was carried out to assess mitochondrial capacity as described in Table 1.

Flux control ratios were calculated to determine the proportion of maximal oxidative phosphorylation (OXPHOS) that

could be supported by the F pathway via β -oxidation (FCR_F; Eq. 1) and by the N pathway via complex I (FCR_N; Eq. 2), as well as the relative capacity to support OXPHOS using octanoyl-carnitine and malate as substrates compared with pyruvate and malate (FCR_{FA/P}; *Eq. 3*). Mitochondrial OXPHOS coupling efficiency (OCE; Eq. 4) was also calculated as a measure of the proportion of OXPHOS not limited by LEAK-state respiration.

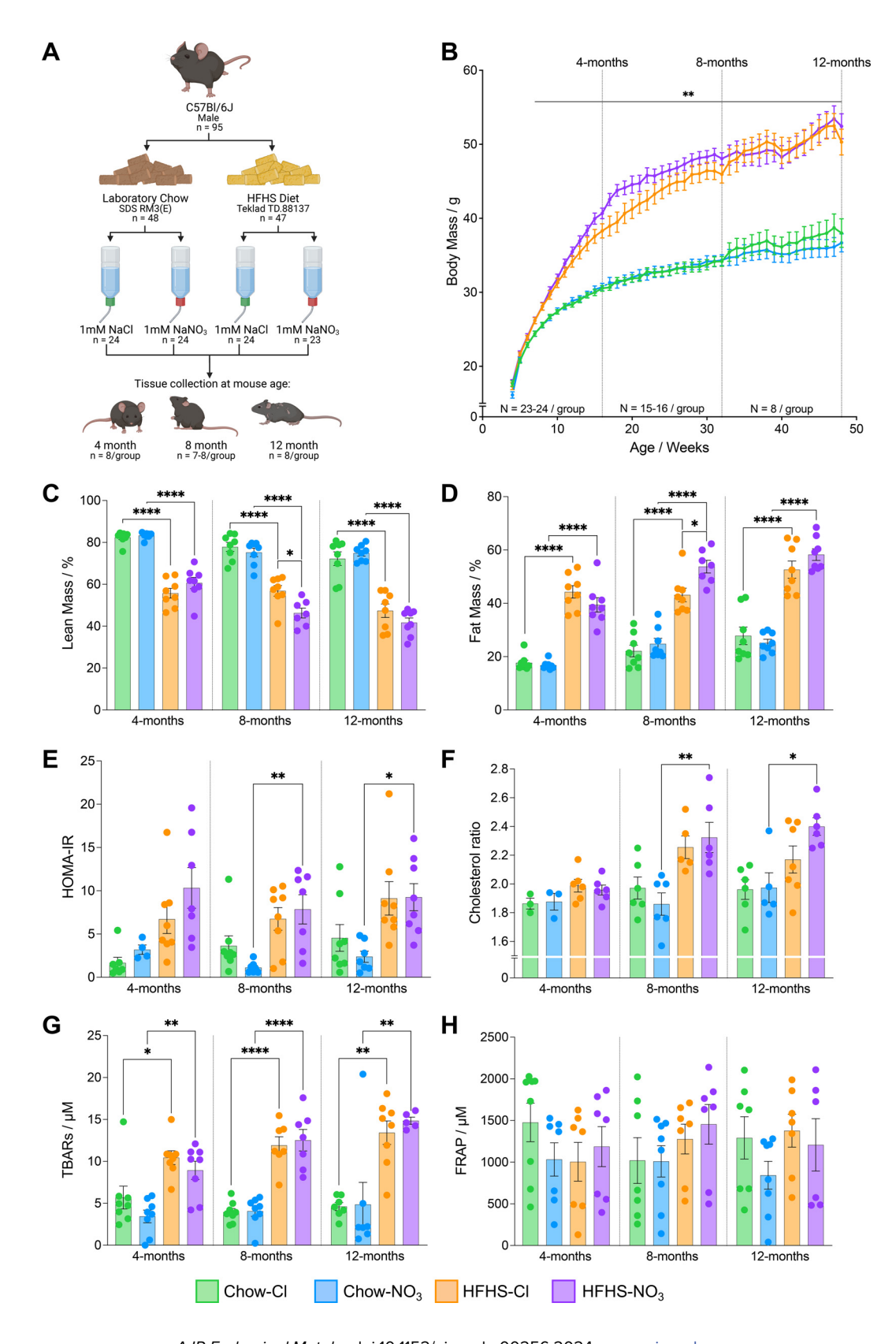


Table 1. Substrate-uncoupler-inhibitor titration used to investigate mitochondrial capacity in permeabilized heart fibers, skeletal muscle fibers, and liver homogenate

		Concentration, mM				
Substrate	Heart	Liver	Skeletal Muscle	Respiratory State		
Malate	1	1	1	OctM _L		
Octanoyl-carnitine	0.5	0.2	0.2			
ADP	10	10	10	OctM _P		
Pyruvate	25	25	25	OctPM _P		
Glutamate	10	10	10	GM_P		
Cytochrome c	0.01	10	0.01			
Succinate	10	10	10	GMS_P		
FCCP*		0.0005 titers	0.00025 titers	GMS _E		
Rotenone	0.0005	0.0005	0.0005	S_E/S_P^**		

Two types of skeletal muscle (gastrocnemius and soleus) were assayed, using the same titration protocol. Cytochrome c was added as a quality control to check outer mitochondrial membrane integrity. *Carbonyl cyanide-p-trifluoromethoxyphenylhydrazone (FCCP) was titrated in the indicated quantities until the maximum rate was reached. No FCCP was added in the heart, as there was no reserve capacity measurable above maximal oxidative phosphorylation (OXPHOS) stimulated following saturation of the electron transport system (ETS) with glutamate and succinate. **In the heart assay, because of the absence of the uncoupler FCCP, addition of the complex I inhibitor rotenone led to measurement of OXPHOS supported by succinate via ETS complex II alone (state Sp), whereas in liver and muscle the uncoupling of the ETS from ATP synthase meant that the oxygen consumption rate measured reflected capacity of ETS complex II (state S_E).

$$FCR_F = \frac{OctM_P}{GMS_P}$$

$$FCR_{N} = \frac{GM_{P}}{GMS_{P}} \tag{2}$$

$$FCR_{FA/P} = \frac{OctM_P}{OctPM_P}$$
 (3)

$$OCE = \frac{OctM_P - OctM_L}{OctM_P}$$
 (4)

Liquid Chromatography-Mass Spectrometry-Based **Metabolite Analyses**

Aqueous and organic metabolites were extracted from ~25 mg of liver LLL or cardiac left ventricle with a modified Bligh and Dyer method (57), as previously described (58), dried under nitrogen, and stored at -80°C until analysis.

For analysis of cardiac glycogenesis intermediates, half the aqueous fraction was reconstituted for hydrophobic interaction liquid chromatography (HILIC), which was performed as previously described (59) with Vanguish UHPLC + series coupled to a TSQ Quantiva Triple Quadrupole Mass Spectrometer (both Thermo Scientific). Identification of detected metabolites was performed by targeted analysis of parent/ daughter ion mass-to-charge ratio (m/z) and retention times

from chemical standards: glucose: $+179.000 \rightarrow +89.000$, 2.6 min; glucose-6-phosphate: $+259.000 \rightarrow +97.077$, 4.0 min; glucose-1-phosphate: $+259.000 \rightarrow +97.077$, 3.9 min; UDP-glucose: $+565.078 \rightarrow +323.000$, 3.88 min.

Analysis of acyl-carnitines in liver and heart was carried out using a reconstituted mix of half of each of the aqueous and organic phases, as previously described (56). Acyl-carnitine analysis was carried out on the same instrumentation as HILIC analysis, with data collection and processing in both cases carried out with Xcalibur software (v.2.2; Thermo Scientific; RRID:SCR_014593).

Open-profiling lipidomics was carried out as previously described (58) with lipid data collected using the Fourier transform mass spectrometer analyzer set in profile mode with a resolution of 60,000 (Ultimate 3000 UHPLC system coupled to an LTQ Orbitrap Elite Mass Spectrometer; both Thermo Fisher Scientific). A full scan was performed across an m/z range of 110–2,000. Lipid metabolites were processed as previously described (58), with peaks identified by XCMS software (RRID: SCR_015538) (60) based on an approximate chromatographic peak detection [full width at half-maximum (FWHM)] of 5 s and a signal-to-noise threshold ratio of 5. Peaks were annotated by accurate mass, with an automated in-house R script and by comparison to the LipidMaps database (61).

All data were normalized to the intensity of appropriate internal standards and to sample protein concentration

Figure 1. Mice fed a high-fat, high-sucrose (HFHS) diet show progressive diet-induced obesity. A: experimental design. Male C57Bl/6J mice were randomly allocated to receive either standard laboratory chow [Special Diet Services RM3 (E)] or HFHS (Teklad TD.88137) from 4 wk of age. Simultaneously, mice were randomized to receive either sodium chloride (NaCl; 1 mM) or sodium nitrate (NaNO₃; 1 mM) via their drinking water. Mice continued to receive these dietary interventions ad libitum until they reached 4, 8, or 12 mo of age, when tissues were collected for subsequent metabolic analyses (n = 7 or 8/group). Created with BioRender.com. B: mouse body mass over the course of the study. Individual mouse body mass was measured once per week. **P < 0.01, HFHS compared with chow-fed groups supplemented with the same water treatment, for each week [2-way ANOVA with Benjamini-Hochberg false discovery rate (FDR) correction and Tukey's post hoc honest significant difference (HSD) test]. C: percentage (%) of the body carcass (after removal of the heart and liver) that represents lean mass determined via dual-energy X-ray absorptiometry. N = 7 or 8/group. D: percentage (%) of the body carcass (after removal of the heart and liver) that represents fat mass determined via dual-energy X-ray absorptiometry. N = 7 or 8/group. E: homeostatic model of insulin resistance (HOMA-IR) calculated according to Ref. 43 using measurements of fasted blood glucose and insulin. N = 4-8/group. F: cholesterol ratio (total cholesterol/HDL cholesterol), used clinically as a predictor of cardiovascular disease (44), calculated from clinical biochemistry measurements. N = 3-7mice/group. G: concentration of thiobarbituric acid reactive substances (TBARS) in plasma, as an indication of levels of lipid peroxidation. N = 5-8 mice/ group. H: ferric reducing ability of plasma (FRAP), as an indication of the antioxidant capacity of plasma. (N = 6-8 mice/group). For C-H, data represent means \pm SE. *P < 0.05, **P < 0.01, ****P < 0.0001; 2-way ANOVA with Tukey's post hoc HSD test for multiple comparisons.

(Pierce BCA Assay; Thermo Scientific) to account for differences in sample size.

Reverse Transcription-Quantitative PCR

Total RNA was extracted from ∼30 mg of liver LLL or ~25 mg of cardiac left ventricle with an RNeasy Fibrous Tissue Mini Kit (QIAGEN Ltd., Manchester, UK) according to the manufacturer's instructions. RNA (1 µg, quantified via NanoDrop 2000 spectrophotometer) was transcribed to cDNA with the QuantiTect Reverse Transcription kit (QIAGEN) and stored at -20°C before analysis. Real-time qPCR was carried out with a LightCycler 480 System (Roche) fitted with a 384-well block, using the QuantiNova SYBR Green PCR kit (QIAGEN) and QuantiTect primer assays (QIAGEN; Supplemental Table S1). Expression was determined in triplicate from each biological replicate. Fold change in gene expression was determined by the relative standard curve method, with expression of all genes normalized to the geometric mean of three housekeeping genes: Rn18s, Srsf4, and Hmbs in liver and Actb, Ywhaz, and Rn18s in heart.

Histology

Sections were fixed in PFA (cardiac midsections) or formalin (LLL and intestinal sections) and embedded into paraffin blocks by standard laboratory methods. For LLL sections, tissue was processed at the Histopathology Core (MRC Metabolic Diseases Unit, Cambridge). All tissue was sectioned at 7 µm with an RM2235 Microtome (Leica Biosystems).

Liver and intestinal morphology was determined via hematoxylin (no. ab220365, Abcam) and eosin (H&E) staining with standard laboratory protocols. Cardiac and hepatic fibrosis was determined by staining for collagen with picrosirius red (PSR) using 0.1% Direct Red in saturated picric acid (12 g·L⁻¹, no. A2520; AppliChem, Darmstadt, Germany) for 1 h. Cardiac glycogen was stained with periodic acid Schiff (PAS) using 0.5% periodic acid (5 min) and Schiff's reagent (10 min) with nuclei counterstained with hematoxylin. To correct for any PAS staining not due to glycogen deposition, one section from each sample was treated with 0.5% α -amylase (type VI-B from porcine pancreas, \sim 2.5 U/mL) for 20 min before staining. After staining, slides were dehydrated in ethanol, cleared in xylene, and mounted with DPX.

Fix-frozen right lateral lobe was embedded in optimum cutting temperature compound (no. KMA-0100-00A; CellPath) and sectioned at 10 µm in a cryostat (OTFAS-001; Bright Instruments, Luton, UK) at −20°C for histological assessment of hepatic steatosis. Sections were allowed to adhere to slides at room temperature for 10 min before sections were fixed in ice-cold formalin for 10 min. Neutral lipid was stained with oil red O [ORO; 0.3% (wt/vol) in 60% isopropanol] for 20 min. Nuclei were counterstained with hematoxylin. After staining, the slides were mounted in glycerin gelatin at 60°C and coverslips sealed with clear nail varnish once the mountant had set.

Slides were imaged with a NanoZoomer 2.0-RS with images collected with NDP.view2 (v2.9.25; Hamamatsu Photonics, Japan). At least three independent sections per biological replicate were examined and analyzed. To determine the level of hepatic pathology, a MASLD activity score (MAS) was generated for each section using sections blinded for experimental condition (Supplemental Table S2) (62). Quantification of villus length was carried out manually in NDP.view2, with 10 intact villi measured per quadrant per intestinal section (63). Quantification of PSR and PAS in cardiac sections was determined after color deconvolution in ImageJ (RRID: SCR_003070) (64). PAS staining was corrected for that in control sections treated with α -amylase to account for any nonglycogen PAS staining.

Statistics

All data are presented as means ± standard error, unless otherwise stated, with differences accepted as statistically significant when P < 0.05. All univariate statistical tests were carried out in R (48) with graphs produced in Prism (v.10.0.3; GraphPad Software LLC., Boston, MA; RRID: SCR_002798). Multivariate statistical analysis was carried out with SIMCA-17 (Umetrics; Sartorius Stedim Data Analytics AB, Umeå, Sweden). Unless otherwise stated, statistical analysis was carried out in line with two a priori questions outlined before commencing the study: 1) at each time point, is there an effect of diet or nitrate supplementation? and 2) is there an effect of diet or nitrate supplementation on age-related and/or disease progression? For each question, two-way ANOVAs were carried out on the relevant experimental cohorts as appropriate, with correction for false discovery rates as required (Supplemental Fig. S1). When significant interactions were found, Tukey's post hoc honestly significant difference (HSD) test was used to consider relevant interactions (Supplemental Fig. S1).

RESULTS

Whole Body Metabolic Phenotype

Mice fed a HFHS diet developed obesity that persisted throughout the 44 wk of the study (Fig. 1B). After 3 wk on the respective diets HFHS-fed mice were 4.6% heavier than chow-fed mice (P < 0.01), and by 12 mo of age HFHS-fed mice were 37.6% heavier than their counterparts on the control chow diet (P < 0.0001; Fig. 1B). There was no effect of nitrate supplementation on body mass (Fig. 1B).

Food intake remained constant throughout the study, with chow-fed mice consuming 4.0 ± 0.03 g·mouse⁻¹·day⁻¹ and HFHS-fed mice eating 3.1 ± 0.05 g·mouse⁻¹·day⁻¹. However, as the HFHS diet was more calorie dense, there was no significant difference in energy intake between the experimental groups throughout the study (Table 2). HFHS-fed mice drank 27.9% less water per day (P < 0.01; Table 2) compared with chow-fed control mice, likely because of the higher sodium content of the latter diet (0.3% in HFHS vs. 10% in chow diet). Despite this, mice receiving drinking water supplemented with 1 mM NaNO₃ had a fivefold higher intake of nitrate compared with NaCl-supplemented control mice (P < 0.0001; Table 2). This resulted in a plasma nitrate concentration that was 1.9-fold higher than in NaCl-supplemented control mice at 4 and 8 mo of age (P < 0.05; Table 3). Circulating nitrite concentrations were significantly elevated only in 4-mo-old mice fed standard rodent chow (Table 3). At 12 mo



Table 2. Food, water, and NO₃⁻ intake across the experimental groups

	Food Intake, kcal mouse ⁻¹ day ⁻¹	Water Intake, mL·mouse ^{−1} ·day ^{−1}	NO ₃ Intake, mg·mouse 1.day 1
Chow/chloride	14.5 ± 0.1	5.8 ± 0.1	1.4 ± 0.0
Chow/nitrate	14.1 ± 0.1	5.3 ± 0.1	12.4 ± 0.2 + + + +
HFHS/chloride	13.8 ± 0.2	4.1 ± 0.1**	1.9 ± 0.1
HFHS/nitrate	14.9 ± 0.2	3.9 ± 0.1**	$8.2 \pm 0.2 **** + + + + +$

Values were calculated based on individual cage measurements (n = 3 or 4 mice/cage; 6 cages/group). Nitrate intake represents combined intake from supplemented water and food (using values provided from the diet suppliers). HFHS, high-fat, high-sucrose diet. Data show means \pm SE. ** \dot{P} < 0.01, ****P < 0.0001, compared with chow-fed mice receiving the same water treatment; $+\dot{T}+P$ < 0.0001, compared with chow-fed mice receiving the same water treatment. pared with chloride-supplemented mice receiving the same diet; 2-way ANOVA with Tukey's honestly significant difference (HSD) post hoc test for multiple comparisons.

there were no differences in plasma nitrate levels between any of the experimental groups (Table 3).

The greater body mass observed in HFHS-fed mice compared with chow-fed mice was reflected in a greater body fat percentage and, correspondingly, a lower lean body mass percentage (P < 0.0001; Fig. 1, C and D). Body fat was ~ 2 - to 2.5-fold greater, whereas lean mass was approximately onethird less in mice fed a HFHS diet, compared with chow-fed control mice. In the 8-mo cohort, HFHS-fed mice also receiving NaNO₃ had 31.3% more body fat and 13.3% less lean mass compared with chloride-supplemented counterparts on the HFHS diet (P < 0.05), although this exacerbation of obesity in nitrate-fed mice was not seen at 12 mo (Fig. 1, C and D).

Mice fed a HFHS diet had a fasted blood glucose concentration that was 36.7% higher than that of chow-fed mice across all ages assessed (P < 0.01), with no difference in fasted plasma insulin concentration (Table 3). Accordingly, HFHS-fed mice had approximately twofold higher HOMA-IR scores indicating evidence of insulin resistance, which reached statistical significance in mice supplemented with

Table 3. Clinical biochemistry measurements and other plasma parameters

	Mouse Age, mo	Chow-Cl	Chow-NO ₃	HFHS-CI	HFHS-NO ₃
Glucose, mmol·L ⁻¹	4	5.7±0.3	6.2 ± 0.2	8.3 ± 0.4**	8.7 ± 0.7**
(n = 7 or 8)	8	6.8 ± 1.1	5.8 ± 0.4	7.9 ± 1.7	8.9 ± 1.5***
	12	6.5 ± 1.2	5.6 ± 0.5	8.5 ± 1.1***	$7.8 \pm 0.6***$
Insulin, mg·L ⁻¹	4	0.19 ± 0.07	0.37 ± 0.07	0.53 ± 0.11	0.77 ± 0.14
(n = 4-8)	8	0.39 ± 0.07	0.14 ± 0.03	0.59 ± 0.12	0.59 ± 0.12
,	12	0.48 ± 0.16	0.29 ± 0.08	0.76 ± 0.18	0.81 ± 0.13
FFA, mmol·L ⁻¹	4	1.8 ± 0.10	1.1 ± 0.10+	1.1 ± 0.10*	1.4 ± 0.08
(n = 2-8)	8	1.6 ± 0.07	1.4 ± 0.10	1.1 ± 0.10*	1.2 ± 0.06
,	12	$0.9 \pm 0.06 \pm 1$	1.4 ± 0.10+	0.8 ± 0.05	$0.8 \pm 0.10 ** \pm 1$
TAG, mmol·L ⁻¹	4	0.80 ± 0.01	0.93 ± 0.01	0.84 ± 0.05	0.83 ± 0.08
(n = 3-7)	8	0.99 ± 0.04	1.10 ± 0.07	0.87 ± 0.04	0.88 ± 0.02**
,	12	0.87 ± 0.11	0.83 ± 0.04	0.72 ± 0.04	0.74 ± 0.04
Cholesterol, mmol·L ⁻¹	4	2.4 ± 0.1	2.6 ± 0.0	5.7 ± 0.2**	5.1 ± 0.6*
(n = 3-7)	8	2.6 ± 0.2	2.4 ± 0.1	6.0 ± 0.8***	7.1±0.5****
· · /	12	2.7 ± 0.1	2.3 ± 0.1	6.5 ± 0.6****	8.6 ± 0.6****†±
HDLc, mmol.·L ⁻¹	4	1.3 ± 0.0	1.4 ± 0.1	2.9 ± 0.2**	2.6 ± 0.3*
(n = 3-7)	8	1.3 ± 0.1	1.3 ± 0.1	2.7 ± 0.4**	3.1±0.2***
,	12	1.4 ± 0.1	1.2 ± 0.1	3.0 ± 0.2****	3.6 ± 0.3****
LDLc, mmol·L ⁻¹	4	0.75 ± 0.08	0.77 ± 0.04	2.4 ± 0.1**	2.1±0.3**
(n = 3-6)	8	0.82 ± 0.09	0.59 ± 0.08	2.9 ± 0.4***	3.5 ± 0.4***
(3 3)	12	0.93 ± 0.07	0.75 ± 0.07	2.9 ± 0.4***	4.2 ± 0.5****†±
ALT, mg⋅mL ⁻¹	4	0.22 ± 0.05	0.26 ± 0.06	0.39 ± 0.08	0.36 ± 0.11
(n = 5-8)	8	0.21±0.03	0.15 ± 0.03	0.40 ± 0.07*	0.44 ± 0.07**
(5 5)	12	0.24 ± 0.04	0.11 ± 0.02	0.47 ± 0.07**	0.54 ± 0.04****
AST, mg⋅mL ⁻¹	4	0.92 ± 0.19	1.01 ± 0.12	1.65 ± 0.56	1.35 ± 0.36
(n = 7 or 8)	8	0.72 ± 0.10	0.59 ± 0.06	1.13 ± 0.17	1.02 ± 0.12
(,, _ , 3, 3)	12	0.76 ± 0.11	0.59 ± 0.11	1.35 ± 0.25	2.04 ± 0.32***
Nitrate, μmol·L ⁻¹	4	32.9±3.7	74.0 ± 7.4†††	27.6±3.2	48.6 ± 4.6**†
(n = 7 or 8)	8	31.7 ± 3.2	51.7 ± 6.8	27.7 ± 3.4	57.4 ± 7.8++
(1 = 7 51 5)	12	49.2 ± 6.1	65.0 ± 10.7	60.2 ± 13.1§	47.5±3.6
Nitrite, μmol·L ⁻¹	4	4.5 ± 0.43	7.9 ± 0.77*	4.6 ± 0.54	6.0 ± 1.74
(n = 7 or 8)	8	3.4 ± 0.53	5.4 ± 0.60	3.7 ± 0.81	4.0 ± 0.99
(11 — 7 01 0)	12	5.4±0.53 5.1±0.52	6.0 ± 1.13	4.9 ± 0.75	3.2 ± 0.42

All clinical biochemistry measurements were assayed from fasted plasma. Nitrate and nitrite concentrations and liver enzymes were measured from terminal blood samples (fed state). Data show means ± SE with numbers of mice assayed indicated. ALT, alanine transaminase; AST, aspartate transaminase; FFA, free fatty acids; HDLc, high-density lipoprotein cholesterol; HFHS, high-fat, high-sucrose diet; LDLc, low-density lipoprotein cholesterol; TAG, triacylglycerols. *P < 0.05, **P < 0.01, ***P < 0.001, ****P < 0.001, compared with chow-fed mice receiving the same water treatment; †P < 0.05, †P < 0.01, ††P < 0.001, compared with chloride-supplemented mice receiving the same diet; $\pm P < 0.01$, compared with 4-mo-old mice within the same treatment group; P < 0.05 compared with 8-mo-old mice within the same treatment group; all statistics represent 2-way ANOVA with Tukey's honestly significant difference (HSD) post hoc test for multiple comparisons.



NO₃⁻ from 8 mo of age compared with their chow-fed counterparts (P < 0.05; Fig. 1E). Total, HDL, and LDL cholesterol were elevated in mice fed a HFHS diet across all ages compared with chow-fed control mice (2.6-fold, 2.1-fold, and 3.7fold higher, respectively; P < 0.05; Table 3). Total and LDL cholesterol were also elevated in the 12-mo HFHS-NO₃ cohort, compared both with the same group at 4 mo of age (69.1% total, 2.1-fold LDL; *P* < 0.01; Table 3) and with the 12mo HFHS-Cl group (30.9% total, 1.5-fold LDL; P < 0.05; Table 3), suggesting an exacerbation of dyslipidemia with longer-term nitrate supplementation. Cholesterol ratio (total/HDL cholesterol) (44) was also elevated in HFHS-NO₃ mice at 8 and 12 mo of age, compared with chow-fed control mice (23.1%; P < 0.05; Fig. 1F) and raised at both of these time points in comparison with 4-mo-old HFHS-NO₃-fed mice (20.2%, P < 0.05; Fig. 1F). There were, however, few clear differences in the plasma free fatty acids or triacylglycerol (TAG) concentrations as a result of age, diet, or nitrate treatment (Table 3).

We also detected elevations in plasma levels of the liver enzymes ALT and AST indicative of liver damage (65). In chloride-supplemented HFHS-fed mice, plasma ALT concentration was 92.4% higher at 8 mo (P < 0.05) and 96.4% higher at 12 mo (P < 0.01) in comparison with chow-fed control mice, whereas in those receiving nitrate plasma ALT concentration was 2.9-fold greater at 8 mo (P < 0.01) and 4.8fold greater at 12 mo (P < 0.0001) compared with chowmatched control mice (Table 3). Plasma AST concentration was also elevated in HFHS-fed mice: in the 8-mo cohort plasma AST was 64.3% higher than in chow-fed mice (P <0.01), whereas at 12 mo HFHS-NO₃-fed mice showed a plasma AST concentration 3.5-fold higher than chow-NO₃ mice (P < 0.001; Table 3).

Quantification of TBARS in plasma showed that, at every time point, lipid peroxidation was higher in HFHS-fed mice compared with chow-fed control mice (2.6-fold; P < 0.05; Fig. 1G), with no effect of nitrate supplementation. This increase in lipid peroxidation was not associated with any differences in plasma antioxidant capacity, as shown by similar FRAP concentrations across all cohorts (Fig. 1H).

Taken together, these data do not support a protective effect of nitrate supplementation for metabolic health during diet-induced obesity.

Whole Body Energy Balance

Next, we sought to determine whether HFHS feeding or nitrate administration altered whole body energy balance, as has been previously reported (66, 67). We used indirect calorimetry and activity measurements to investigate energy utilization in the 12-mo cohort when mice were 10 mo of age (Fig. 2, A-E).

Throughout the 48-h metabolic cage protocol, chow-fed mice had a higher respiratory exchange ratio (RER) than HFHS-fed mice $(0.84 \pm 0.005 \text{ vs. } 0.76 \pm 0.002; P < 0.001)$, which was independent of nitrate supplementation (Fig. 2, A and B), indicating that HFHS-fed mice were more reliant on fat oxidation than their chow-fed counterparts (68). Chowfed mice also showed a greater difference in RER between the peaks and troughs recorded during light and dark periods compared with HFHS-fed mice (Fig. 2, A-C), indicating greater metabolic flexibility to switch between the fed and

fasted states, and this reached statistical significance in NaCl-supplemented mice (47.0% lower in HFHS-Cl mice, P < 0.05; Fig. 2C).

HFHS-fed mice had a total energy expenditure (EE) that was 20.3% greater than mice maintained on the chow diet (P < 0.0001; Fig. 2D), with no effect of nitrate supplementation. When normalized to body mass, however, EE was 11.2% lower in HFHS-fed mice compared with chow-fed mice (P < 0.05; Fig. 2E). Again, there was no apparent effect of nitrate supplementation, although mass-corrected EE was 13.5% lower in the inactive light period in HFHS-NO3 mice compared with chow-fed control mice (P < 0.05; Fig. 2E). Regression analysis demonstrated that EE varied consistently with total body mass across all experimental groups (Supplemental Fig. S2A).

Given the relationship between EE and body mass, we investigated how the HFHS diet might exert an obesogenic effect despite similar caloric intake and EE compared with chow-fed control mice. First, we investigated mitochondrial respiratory capacity in the skeletal muscle, since this is the largest insulin-sensitive tissue in the body (69) and largely dominates the measurement of whole body RER (70). We found very little difference in mitochondrial respiration between cohorts in either soleus (oxidative type I muscle) or gastrocnemius [a more glycolytic type II muscle (71); Supplemental Fig. S2, B and C], with similar OXPHOS coupling efficiencies across treatment groups within given muscle types (Supplemental Fig. 2D).

However, contribution to maximal OXPHOS through the F pathway via β-oxidation (FCR_F) was 38.8% higher in gastrocnemius from 8-mo-old HFHS-NO3 mice compared with chow-fed control mice (P < 0.05; Fig. 2F), and the relative capacity for fatty acid oxidation (FCR_{FA/P}) was also higher in gastrocnemius from HFHS-fed mice compared with chow-fed control mice (26.0% higher in 8-mo-old HFHS-NO₃ mice, 32.6% higher in 12-mo HFHS-Cl mice; P < 0.05; Fig. 2G). These differences were not apparent in soleus (Fig. 2, *F* and *G*).

These findings support a shift in mitochondrial substrate preference in the gastrocnemius of HFHS-fed mice but did not indicate a reduction in overall muscle oxidative capacity or altered mitochondrial efficiency.

Next, we investigated whether the HFHS diet resulted in changes in intestinal morphology similar to those previously reported to result from dietary fructose (44). Accordingly, a cohort of mice fed the HFHS diet for 8 wk showed longer villi across the small intestine and deeper colonic crypts than chowfed control mice (62.8%, *P* < 0.0001; Fig. 2*H*, Supplemental Fig. S2E). This suggests that obesity in the HFHS-fed mice resulted from increased nutrient absorption rather than increased intake or reduced expenditure.

Cardiac Metabolism and Fibrosis

As ~65% of diabetes-related mortality arises from cardiovascular diseases (72), with alterations in myocardial metabolism considered central to the etiology (73), we sought to investigate whether inorganic nitrate supplementation altered cardiac metabolic function in HFHS-fed mice. There was no difference in either heart mass (Supplemental Fig. S3A) or heart mass normalized to tibia length (a proxy for body size) (74) as a result of age, diet, or nitrate supplementation (Fig. 3A).

Cardiac glycogen content was assessed in sections of cardiac midsection with PAS staining (Fig. 3, B and C). When corrected for staining in the presence of α -amylase, the hearts of 12-mo-old HFHS-fed mice showed 3.0-fold higher PAS staining than those of age-matched chow-fed control mice (P < 0.0001), indicative of increased glycogen content (Fig. 3C). The area staining positively for PAS was also 82.5% higher in the HFHS-Cl cohort than the HFHS-NO₃ cohort at 12 mo of age (P < 0.01; Fig. 3C), indicating that glycogen accumulation was prevented when mice were supplemented with nitrate.

Using HILIC-mass spectrometry, we quantified metabolites involved in glycogen synthesis in the left ventricle (Fig. 3, D-G). HFHS-fed mice had 59.6% higher cardiac glucose levels compared with chow-fed control mice across all cohorts (Fig. 3D), which may be due to the high sucrose content of the diet. Cardiac glucose-6-phosphate showed no difference across age, diet, or nitrate supplementation (Fig. 3E); however, glucose-1-phosphate levels were 60.3% lower in hearts from HFHS-NO₃ mice compared with HFHS-Cl mice at 4 mo of age (P < 0.05; Fig. 3F). Glucose-1-phosphate levels in HFHS-Cl fed mice, however, showed decreasing levels with age (Fig. 3F), being 33.2% lower in 8-mo-old mice compared to 4-mo-old mice and 73.5% lower in 12-mo-old mice fed HFHS-Cl (P < 0.05; Fig. 3F). There was no difference in cardiac levels of UDP-glucose as a result of diet or nitrate supplementation (Fig. 3G).

The expression of genes involved in glycogen synthesis was unaffected by diet or nitrate supplementation (Fig. 3, H-J); however, both glycogen synthase 1 (Gys1) and Ppp1ca (1 of the catalytic subunits of protein phosphatase 1) showed lower expression in the hearts of older HFHS-fed mice. In HFHS-fed mice receiving NaCl, Gys1 expression was 50.2% lower (P < 0.05; Fig. 3H) and Ppp1ca was 51.8% lower (P <0.01; Fig. 3I) at 12 mo than at 4 mo. However, in HFHS-NO₃fed mice, lower expression was detectable in the 8-mo cohort, with *Gys1* expression 54.5% lower at 8 mo (*P* < 0.001) and 61.8% lower at 12 mo (P < 0.0001) compared with hearts from 4-mo-old mice (Fig. 3H) and Ppp1ca expression 42.8% lower at 8 mo (P < 0.05) and 56.5% lower at 12 mo (P < 0.001) compared with that at 4 mo (Fig. 3I). There were no differences in cardiac expression of Gsk3a as a result of age or disease progression (Fig. 3*J*).

Taken together, these findings suggest that nitrate supplementation minimizes glycogen accumulation as a result of long-term HFHS feeding. Glycogen accumulation, which can occur in the diabetic heart (75), has been linked to the cardiometabolic stress response (76).

We next investigated myocardial fat metabolism, given that fatty acids are the predominant source of ATP in the healthy heart (77) and alterations in substrate usage are canonical markers of both the diabetic and failing heart (73, 78). Total TAG content of the left ventricle [as determined by liquid chromatography-mass spectrometry (LC-MS) peak intensity] was 1.5-fold higher in HFHS-fed mice compared with chow-fed control mice, reaching statistical significance in 4and 8-mo chloride-supplemented mice (P < 0.05; Fig. 4A). Similarly, total cardiac diacylglycerol (DAG) was 53.1% higher in HFHS-Cl mice at 4 mo and 79.8% higher at 8 mo compared with chow-fed control mice (P < 0.0001; Fig. 4B). HFHS-NO₃-fed mice showed no differences in cardiac DAG levels compared with either HFHS-Cl or chow-NO₃-fed mice at any age.

Moreover, combined HFHS-NO₃ feeding prevented a reduction in the total acyl-carnitine pool that was observed in hearts from mice fed HFHS-Cl at 4 mo (-21.2%, P < 0.05) and 12 mo (-35.2%, P < 0.01) compared with chow-fed control mice (Supplemental Fig. S3B). However, HFHS feeding resulted in alterations to the composition of the cardiac acyl-carnitine pool, independent of nitrate supplementation (Fig. 4, C and D; Supplemental Fig. S3C), including a relative depletion in the contribution of short-chain (total carbons C2-C5) acyl-carnitines to the total cardiac carnitine pool and a higher contribution of long-chain acyl-carnitines (total carbons >C13) to the total cardiac carnitine pool in 4- and 8-mo-old mice (P < 0.05; Fig. 4C). Medium-chain acyl-carnitines (total carbons C6–C12) were higher in HFHS-fed mice, regardless of age or nitrate supplementation (P < 0.01; Fig. 4, C and D).

To investigate whether these changes in metabolites were reflected in mitochondrial capacity, we investigated cardiac mitochondrial respiratory function in saponin-permeabilized fiber bundles. We found no differences in mass-specific respiration in any state assayed due to diet, nitrate, or age (Supplemental Fig. S3D). However, at 12 mo relative contribution of fatty acid oxidation (FCR_F) was 13.9% higher in the hearts of HFHS-fed mice than those of chow-fed mice regardless of nitrate supplementation (P < 0.01; Fig. 4E). The capacity for fatty acid oxidation relative to pyruvate oxidation (FCR_{FA/P}) was also higher in the hearts of 12-mo-old HFHS-fed mice: HFHS-Cl-fed mice had 11.8% higher FCR_{FA/P} compared with chow-Cl mouse hearts (P < 0.05), whereas HFHS-NO₃ mice had a 20.9% higher cardiac FCR_{FA/P} than chow-NO₃ mice (P < 0.05; Fig. 4F).

We also investigated cardiac fibrosis histologically in cardiac midsections, using picrosirius red (PSR) staining for collagen (Fig. 4G). Analysis of the area staining positive for collagen showed that, at all ages, HFHS-NO₃-fed mouse hearts had a 71.7% higher cardiac collagen content than chow-fed control mice (P < 0.01; Fig. 4H). At 8 mo, hearts from HFHS-NO₃ mice also showed a collagen content that was 45.4% higher than that of hearts from HFHS-Cl mice (P < 0.05). This trend of higher collagen content in HFHS-NO₃ mouse hearts compared with HFHS-Cl mice was also seen at 4 mo (40.9% higher; P =0.0624) and 12 mo (23.8% higher; P = 0.107; Fig. 4H).

In summary, inorganic nitrate supplementation exerted a metabolic benefit in the HFHS-fed mouse heart, through minimizing cardiac lipid accumulation and delaying glycogen accumulation, but did not affect mitochondrial respiratory capacity and resulted in increased cardiac fibrosis from 4 mo.

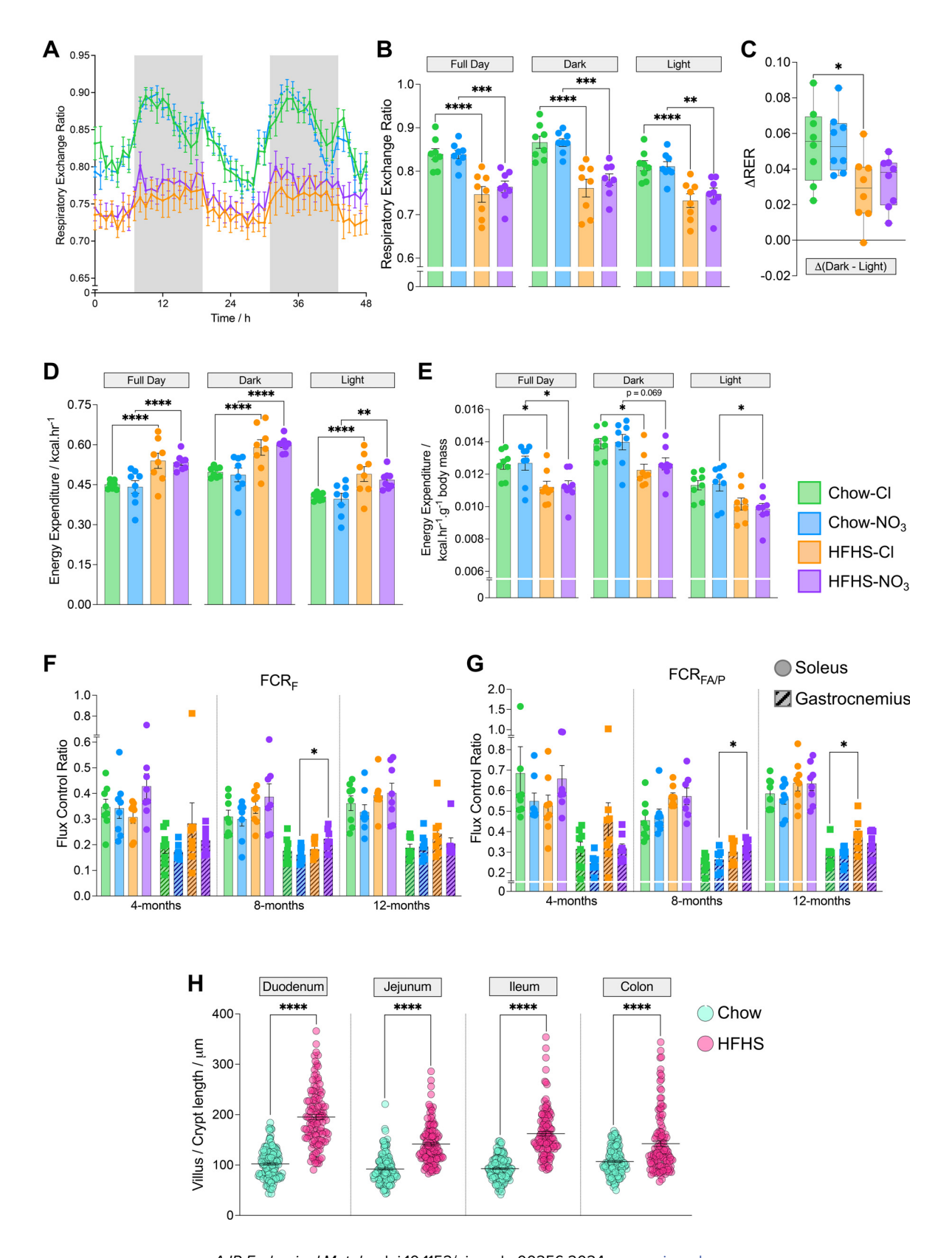
Inorganic Nitrate and MASLD Progression

A common, silent comorbidity of obesity is MASLD (79). We therefore investigated the effect of inorganic nitrate supplementation on liver metabolism and MASLD progression in HFHS-fed mice.

At 12 mo, mice fed a HFHS diet had livers that were 1.8-fold larger (relative to body mass) than chow-fed control mice (P < 0.0001; Fig. 5A). Interestingly, HFHS-NO₃-fed mice showed greater hepatomegaly than HFHS-Cl-fed mice (total liver mass being 1% heavier relative to body weight, P < 0.05; Fig. 5A). HFHS-NO₃ mice also had a greater prevalence of tumors, with 50% of this group having visible tumors on the liver surface, compared to only one mouse in the HFHS-Cl group and none in chow-fed mice $[\chi^2(df = 3, N = 32) = 10.2,$

P < 0.05; Fig. 5B].

As hepatocellular carcinoma (HCC) is a known consequence of MASLD, we investigated transcriptional markers of HCC (80, 81) in livers across all cohorts (Fig. 5, *C–E*). *Akr1b10*, a marker positively associated with HCC progression, was





elevated in 12-mo-old HFHS-fed mice compared with chowfed control mice irrespective of nitrate supplementation (4.7fold, P < 0.01; Fig. 5C). Moreover, HFHS-NO₃-fed mice showed specific elevation of the HCC marker *Spp1*, which was 3.2-fold higher than in chow-fed mice at 8 mo of age (P <0.01) and by 12 mo showed expression that was 11.1-fold higher than in chow-fed control mice (P < 0.0001) and 2.4fold higher than HFHS-Cl-fed mice (p < 0.01; Fig. 5D). Hepatic *Spp1* expression also showed a progressive increase in HFHS-NO₃-fed mice, with 8.6-fold higher (P < 0.0001) and 3.3-fold higher (P < 0.001) expression at 12 mo compared with 4 and 8 mo, respectively (Fig. 5D). Furthermore, Hrg (a marker negatively associated with HCC) was lower in livers of HFHS-NO₃-fed mice from 8 mo of age, reaching significance in the 12-mo cohort compared with chow-fed control mice (61.7%, p < 0.05; Fig. 5E). Hrg expression was also 64.7% lower in 8mo-old mice (P < 0.01) and 77.2% lower in 12-mo-old mice (P < 0.0001) fed a HFHS-NO₃ diet, compared with the same cohort at 4 mo old (Fig. 5E).

We further undertook blind histological scoring of MASLD activity (MAS) in livers from mice of all cohorts (Fig. 5, F–I). Representative histological images are shown in Fig. 5, F-H. Mice fed a HFHS diet had livers with MAS that were, on average, 4.46 points higher than those maintained on chow (P <0.001), independent of nitrate supplementation (Fig. 51).

As the steatotic component of MAS was graded 2.1 points higher in HFHS-fed mice compared with chow-fed control mice at every time point (P < 0.0001; Supplemental Fig. S4A), hepatic lipid content was quantified to more accurately examine differences in hepatic lipid load across the experimental cohorts (Fig. 5J). Whereas HFHS-fed mice showed clear steatosis with 4.4-fold more fat per gram liver tissue compared with chow-fed control mice (P < 0.01; Fig. 5*J*), inorganic nitrate supplementation did not alter the steatotic component of MASLD.

In contrast, expression of the fibrotic markers Serpine1 and Pdgfb indicated that fibrosis may be elevated at an earlier stage in HFHS-NO₃-fed mice compared with HFHS-Cl mice (Fig. 5, K and L). Whereas Serpine1 expression was elevated 20.0-fold in livers from HFHS-Cl-fed mice at 12 mo compared with chow-fed control mice, there was no difference in expression of Serpine1 in HFHS-Cl and chow-Cl livers from younger mice (Fig. 5K). In HFHS-fed mice supplemented with NO₃⁻, however, Serpine1 showed a 6.7-fold higher expression at 8 mo (P < 0.05) and 8.5-fold higher expression at 12 mo (P = 0.0532) compared with chow-fed control mice (Fig. 5K). Likewise, Pdgfb expression was 3.1fold higher at 8 mo (P < 0.01) and 13.3-fold higher at 12 mo (P < 0.05) in the livers of HFHS-Cl mice compared with those

of chow-Cl mice, whereas in HFHS-NO₃-supplemented mice Pdgfb showed a 3.6-fold higher expression at 8 mo (P < 0.0001) and 13.2-fold higher expression at 12 mo (P < 0.01) compared with chow-fed control mice (Fig. 5L).

Taken together, these data suggest that nitrate supplementation accelerates MASLD progression in HFHS-fed mice, including greater incidence of hepatocellular carcinoma. Although nitrate did not alter steatosis, fibrosis was initiated earlier in HFHS-NO₃ livers than in those of HFHS-Cl mice.

Hepatic Lipid Metabolism and Mitochondrial Function

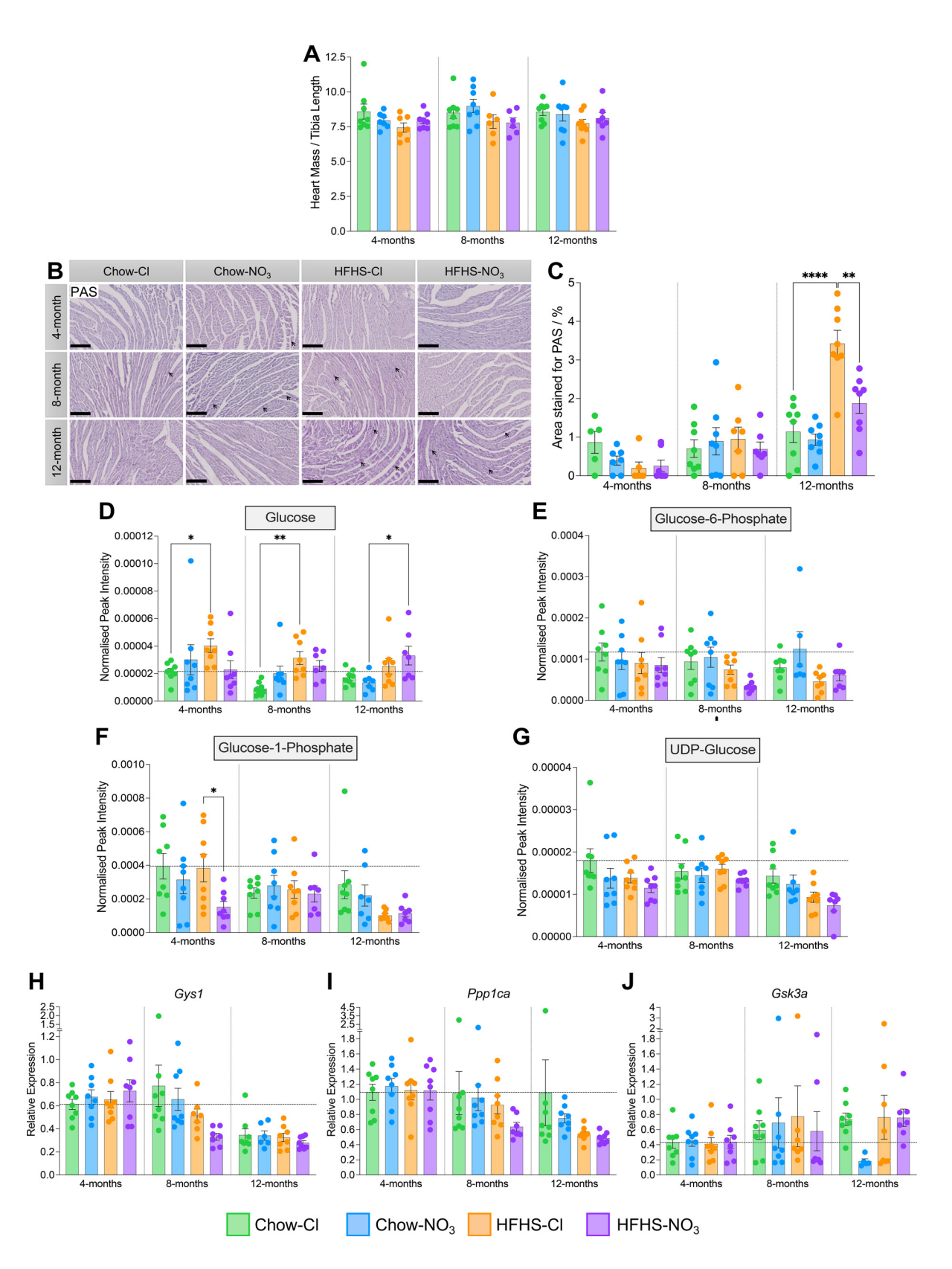
Finally, given the changes in steatosis in HFHS-fed mice, we sought to investigate whether the lipidome and, subsequently, fat metabolism were altered in mice fed a HFHS diet or inorganic nitrate. Open-profiling lipidomics identified >900 lipid species present in the livers of mice across all experimental conditions and time points. Principal component analysis (PCA) revealed that the hepatic lipidomes of HFHS-fed mice were distinct from those of chow-fed mice $[R^2X_{(\text{cum})} = 88.3\%, Q^2_{(\text{cum})} = 82.2\%]$, irrespective of nitrate (Supplemental Fig. S4B). Plotting all lipids by species indicated clear differences due to diet in the phosphatidylserine (PS) and TAG complements of the lipidome (Supplemental Fig. S4C), with more subtle changes due to age and nitrate supplementation also appearing in these classes.

We therefore investigated the changes occurring in the PS and TAG complements in more depth. Partial least squarediscriminant analysis (PLS-DA) of the PS $[R^2X_{(cum)} = 95.3\%,$ $R^2Y_{\text{(cum)}} = 40.2\%$, $Q^2_{\text{(cum)}} = 24.1\%$, P < 0.05; Supplemental Fig. S4D] and TAG $[R^2X_{\text{(cum)}} = 84.6\%$, $R^2Y_{\text{(cum)}} = 28.5\%$, $Q^2_{\text{(cum)}} = 26\%$, P < 0.0001; Supplemental Fig. S4E] complements, respectively, in chloride-supplemented mice revealed that these lipid classes alone were sufficient to discriminate between livers of chow- and HFHS-fed mice. PS species were depleted across the board in livers of mice fed a HFHS diet, independent of nitrate supplementation (Fig. 6A), and although TAGs were generally increased in HFHS-fed mouse livers, there was greatest accumulation of species associated with de novo lipogenesis [total carbons 44 to 48 (82); Fig. 6B]. Interestingly, the top five species differentiating HFHS- from chow-fed livers [by variable importance parameter (VIP) score for both PS and TAGs were highly correlated with the score given for steatosis in MAS (all P < 0.0001; Pearson's correlation). The most highly correlated PS (PS[34:2]; $R^2 =$ 0.7733) and TAG (TG[46:1]; $R^2 = 0.8211$) were 99.9% lower (P < 0.0001; Supplemental Fig. S4F) and 42.3-fold higher (P < 0.0001; Supplemental Fig. S4F), respectively, in livers with histologically classified steatosis (MAS steatosis score

Figure 2. Whole body energy expenditure and skeletal muscle mitochondrial metabolism differences do not account for development of obesity in high-fat, high-sucrose (HFHS)-fed mice. A: changes in respiratory exchange ratio (RER), determined from oxygen consumption (Vo2) and carbon dioxide production (VCO₂). Shaded areas represent the dark period. B: average RER during the dark period, the light period, and across a full day, determined from Vo₂ and Vco₂ in 10-mo-old mice during the 48-h metabolic cage protocol. C: difference in average RER between the active dark period and the quiet light period. D: energy expenditure across the dark period, light period, and full day. E: mass-normalized energy expenditure (normalized to total body mass) across the dark period, light period, and full day. For B-E, N=8 mice/group. *P<0.05, **P<0.001, ****P<0.0001, ****P<0.0001lyzed according to the CalR framework (47) adapted for a 2×2 design. F: contribution of the F pathway via β -oxidation to maximal oxidative phosphorylation (OXPHOS) (FCR_F) in saponin-permeabilized skeletal muscle fibers. G: capacity for OXPHOS supported by octanoyl-carnitine and malate relative to pyruvate and malate (FCR_{FA/P}) in saponin-permeabilized skeletal muscle fibers. For F and G, N = 7 or 8 mice/group. *P < 0.05, 2-way ANOVA with Tukey's post hoc honestly significant difference (HSD) test for multiple comparisons. H: villus length (or colonic crypt depth) across regions of the intestine measured in histological sections (Supplemental Fig. S2D) from mice fed chow or HFHS diet for 8 wk. N=3 or 4 mice/group. ****P<0.0001, unpaired 2-tailed t test with Welch's correction. All data represent means \pm SE.

2 or 3) compared with those without steatosis (MAS steatosis score 0 or 1), suggesting that these lipidomic differences are associated with MASLD not just increased dietary intake of lipid.

We next considered the expression of genes involved in hepatic lipid catabolism and anabolism. Lipogenesis genes were found to be generally upregulated in HFHS-fed mice (Fig. 6, C-E). Fatty acid synthase (Fasn) showed 7.4-fold





higher expression at 4 mo and 5.0-fold higher expression at 8 mo in HFHS-Cl mice compared with chow-fed control mice (P < 0.01; Fig. 6C), with no impact of inorganic nitrate supplementation. Stearoyl-CoA desaturase 1 (Scd1) was expressed 8.1-fold higher in livers from 4- and 8-mo-old HFHS-fed mice regardless of nitrate supplementation (P < 0.05; Fig. 6D). Similarly, acetyl-coA carboxylase (Acc1) was expressed 2.9fold higher in 4- and 8-mo-old HFHS-fed mice (P < 0.05; Fig. 6E) but remained elevated in 12-mo-old HFHS-NO₃ mice, where expression was 3.6-fold higher than in chow-fed control mice (P < 0.05; Fig. 6E). Interestingly, the genes encoding the β-oxidation enzymes 3-hydroxyacyl-CoA dehydrogenase (Hadh) and long-chain acyl-coA dehydrogenase (Acadl) showed an age-dependent expression profile (Fig. 6, F and G). In 4-mo-old HFHS-Cl mice, *Hadh* expression was 4.7-fold higher (P < 0.0001; Fig. 6F) and Acadl expression was 2.2-fold higher (P < 0.01; Fig. 6G) compared with chow-fed control mice. However, there was no difference due to diet or nitrate supplementation in 8-mo-old mice, and by 12 mo-old *Hadh* expression was 60.3% lower in HFHS-NO₃ mice (P < 0.05; Fig. 6F) and Acadl expression was 45.4% lower in HFHS-Cl mice (P < 0.05, Fig. 6G) compared with chow-fed control mice. Chow-NO₃-fed mice also showed 44.0% lower Acadl expression at 12 mo compared with chow-Cl-fed mice (P <0.05: Fig. 6G).

We next investigated the acyl-carnitine profile of the liver. The total acyl-carnitine pool was 40.7% lower in HFHS-fed mice compared with chow-fed mice (Supplemental Fig. S5A). However, as in the heart, there were alterations to the composition of the hepatic acyl-carnitine pool independent of nitrate supplementation (Fig. 6, H and I; Supplemental Fig. S5B). At all time points, relative levels of long-chain (>C13) acyl-carnitines were 3.4-fold higher in HFHS-fed mice (P < 0.05), and 8- and 12-mo-old HFHS-fed mice showed 22.8% lower contribution of free carnitine to the total carnitine pool (Fig. 6H). Surprisingly, there was no concurrent suppression in the relative level of short-chain (C2–C5) acyl-carnitines with the accumulation in long-chain acylcarnitines, except in 12-mo-old HFHS-NO₃ mice, where the relative contribution of short-chain acyl-carnitines to the total carnitine pool was 18.2% lower than in chow-fed control mice (P < 0.01; Fig. 6H). There were no differences in relative levels of medium-chain acyl-carnitines (Fig. 6, H and I).

Finally, we assessed whether changes measured in the liver during MASLD progression were associated with alterations in mitochondrial respiratory function. Generally, mice fed a HFHS diet tended to have a lower mass-corrected respiratory capacity in all states at all ages, independent of nitrate supplementation. This was especially evident with β -oxidation-supported respiration (OctM_L and OctM_P) and after stimulation of complex II with succinate (GMSP, GMSE and S_E; Supplemental Fig. S5C). In line with this, the capacity for fatty acid oxidation relative to pyruvate oxidation (FCR_{EA/P}) was 23.7% lower in the livers of 4-mo-old HFHS-fed mice (P < 0.05) and 30.3% lower in the livers of 8-mo-old HFHS- NO_3 mice (P < 0.01) compared with chow-fed control mice (Fig. 6J). However, the contribution of the N pathway to maximal OXPHOS (FCR_N) was 34.6% higher in 4-mo-old HFHS-fed mice regardless of nitrate supplementation (P < 0.05) and 42.1% higher in 4-mo-old HFHS-NO₃ mice (P < 10.01) compared with chow-fed control mice (Fig. 6K).

Taken together, these results highlight that hepatic lipid metabolism is impacted by HFHS feeding, with metabolic changes occurring early and persisting throughout life in mice fed a HFHS diet.

DISCUSSION

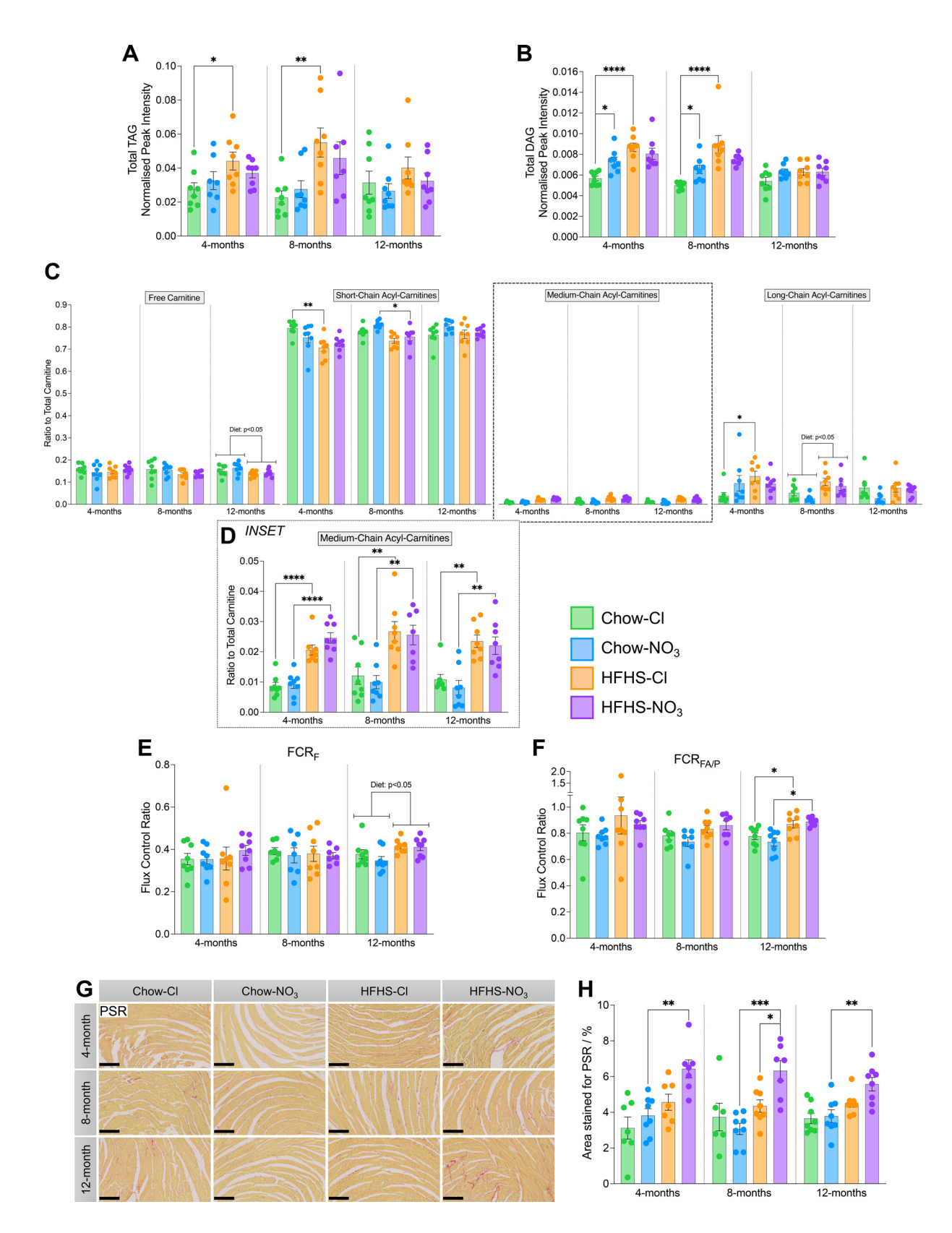
Inorganic nitrate has been suggested as a possible treatment for obesity-related metabolic disease owing to the relative ease of modifying intake through the diet (83) and favorable effects upon acute administration including increased bioavailability of NO (20), improvement of mitochondrial efficiency (66), and enhanced mitochondrial β-oxidation (35). Collectively, these have been proposed to be beneficial in treating metabolic diseases by ameliorating any effects of mitochondrial dysfunction and providing a mechanism for dissipating excess FFA. However, here we show that dietary supplementation with a moderate dose of inorganic nitrate supplementation (achievable in humans via a modest increase in leafy green vegetable consumption) (84) was not effective as a therapeutic intervention in mice with diet-induced obesity and was instead associated with adverse effects in HFHS-fed mice (Fig. 7). Most notably, dietary supplementation with inorganic nitrate resulted in elevated plasma LDL cholesterol, increased cardiac fibrosis, and accelerated MASLD severity in HFHS-fed mice, including a significant, detectable tumor burden in 12-mo-old HFHS-NO3 fed

A major strength of this study is that we have investigated the metabolic phenotype at multiple time points over a sustained time frame. Many studies investigating metabolic alterations bought about by obesity or diabetes consider a single time point in comparison with a healthy control. However, type II diabetes is a progressive disease that exists on a spectrum from mild insulin resistance to overt glucose intolerance with β-cell impairment, and it is therefore important to consider when and where adverse metabolic remodeling occurs as the disease progresses. This temporal analysis has also allowed us to consider some of the longer-

Figure 3. Inorganic nitrate supplementation prevents glycogen accumulation in high-fat, high-sucrose (HFHS)-fed mouse heart. A: heart mass, normalized to tibial length, as a proxy for body size. B: representative cardiac midsections stained with periodic acid Schiff (PAS) stain at ×20 magnification. Scale bars, 150 µm. Glycogen deposits are stained magenta and marked with arrows (maximum 3 per slide shown). C: quantification of area staining positive for PAS. Percentages were corrected for the staining present in control sides pretreated with α-amylase, thereby excluding any staining resulting from other glycans and mucins. D: relative cardiac concentration of glucose, determined by hydrophobic interaction liquid chromatography (HILIC)-mass spectrometry (MS). E: relative cardiac concentration of glucose-6-phosphate, determined by HILIC-MS. F: relative cardiac concentration of glucose-1phosphate, determined by HILIC-MS. G: relative cardiac concentration of UDP-glucose, determined by HILIC-MS. H: relative cardiac expression of Gys1, determined by RT-qPCR. I: relative cardiac expression of Ppp1ca, determined by RT-qPCR. J: relative cardiac expression of Gsk3a, determined by RTqPCR. Data represent means \pm SE; N = 6-8 mice/group. Data in D-G are normalized to an appropriate internal standard and sample protein concentration. For H-J, horizontal line indicates relative expression in 4-mo chow/chloride mice. *P < 0.05, **P < 0.01, ****P < 0.001, 2-way ANOVA with Tukey's post hoc honestly significant difference (HSD) test for multiple comparisons.

term effects associated with nitrate supplementation, which are not apparent over a shorter time frame. Furthermore, we have utilized a range of gold-standard techniques allowing an in-depth dissection of the progressive obesity phenotype alongside changes in mitochondrial function, tissue metabolism, and morphology.

Our findings add clarity to the time course of metabolic derailment occurring over the development of obesity and



related comorbidities. This is evident, for instance, in the liver, where our in-depth analysis of the MASLD phenotype, accompanied with whole lipidome analysis and mitochondrial functional measurements, has allowed a comprehensive assessment of the metabolic changes occurring from a healthy tissue all the way to severe disease. For instance, although PS depletion has previously been shown to occur in metabolic dysfunction-associated steatohepatitis (MASH) patients (85), our data highlight that PS depletion occurs from the very earliest time points of metabolic derailment, before progression to MASH. Furthermore, combined suppression of PSS1 and PSS2 (enzymes involved in the synthesis of PS) lowered hepatic PS in mice and concurrently increased hepatic TAG (86), in agreement with the changes reported here. However, we additionally show that these changes are accompanied by alterations in the balance between hepatic lipid catabolism and anabolism, alongside changes in mitochondrial respiratory function.

Our finding of detrimental consequences of inorganic nitrate in HFHS diet-fed mice (Fig. 7) can be considered alongside previously published benefits of nitrate supplementation in healthy rodents. For instance, up to 17 mo of inorganic nitrate supplementation at an equivalent dose was shown to have no adverse effects in male C57Bl/6 mice and improved fasting insulin in these mice (42); however, these mice were maintained on a standard laboratory chow (with depleted nitrate) (42). The adverse effects observed in the HFHS-NO₃ mice here are likely to result from an interaction between the obesogenic diet and the nitrate itself: indeed, we also observed no adverse effects in nitrate-supplemented mice fed a standard laboratory chow diet. Of note, however, nitrate supplementation did not result in any improvement in fasting insulin in chow-fed mice in our study, contrary to that previously observed (42).

Furthermore, inorganic nitrate has been shown to increase mitochondrial β -oxidation capacity in rat skeletal muscle (35, 87), a finding that gave rise to some of the hypothesized benefits of inorganic nitrate supplementation in obesity-related comorbidities. However, this effect was not observed in NO₃supplemented mice here, regardless of whether they received standard chow or HFHS diet or whether soleus or gastrocnemius muscle was analyzed. This apparent discrepancy is likely due to the lower baseline nitrate levels of rats in comparison to mice (88), resulting in reduced elevations in plasma nitrate levels achievable in mice, as used in this study, through dietary supplementation with NaNO₃. Although plasma levels of nitrate in rats are more similar to those in humans (88, 89), one of the significant advantages of this work was that by using mice rather than rats a long-term study could be carried out (90), allowing us to

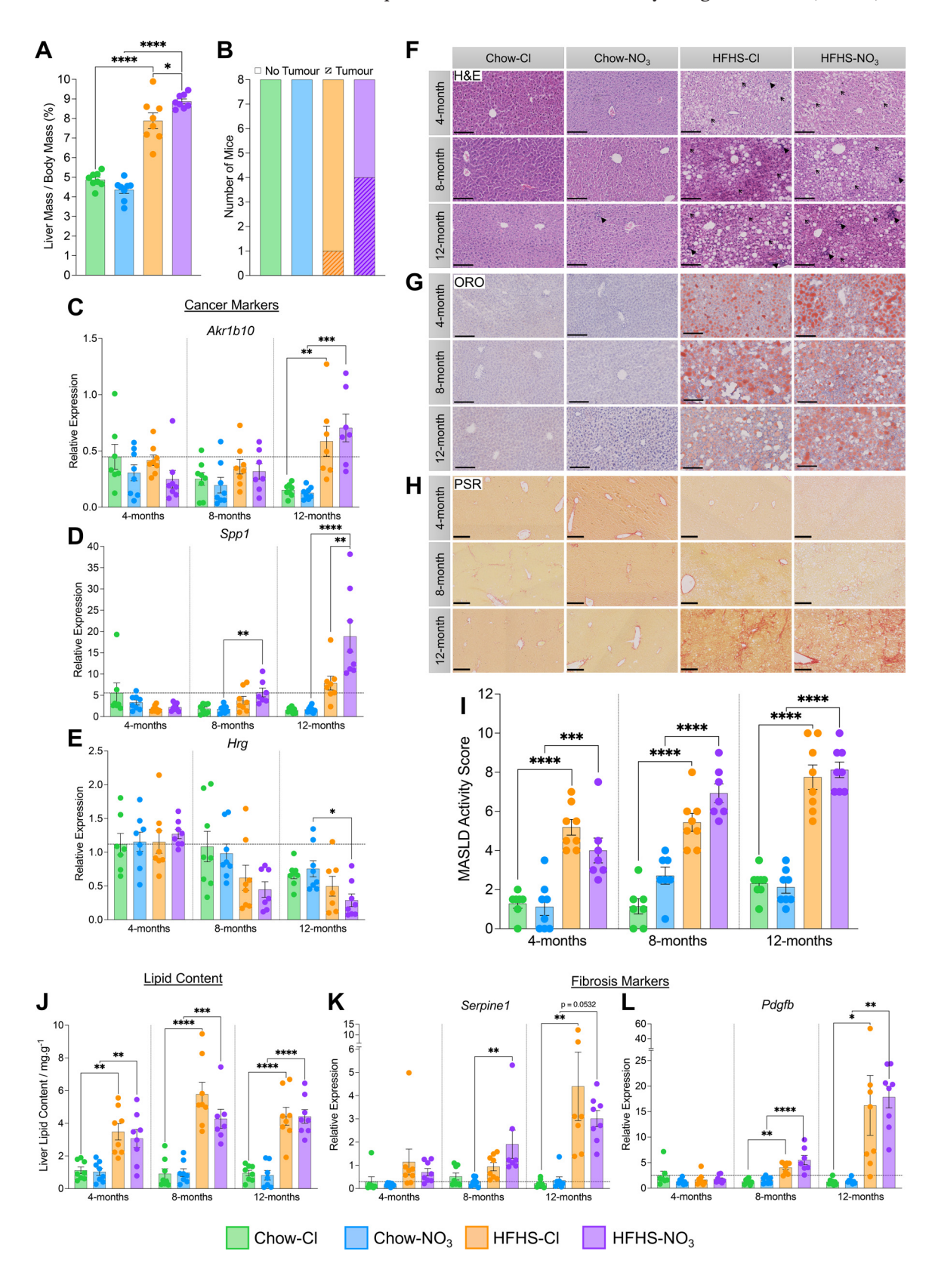
observe the metabolic alterations over the entire course of obesity progression.

There may also be alternative explanations for the lack of an apparent beneficial effect of nitrate supplementation in this study. For instance, given that commensal oral microbes are vital for the reduction of NO₃⁻ to NO₂⁻ (18), alterations to the oral microbiome are known to affect NO production from inorganic nitrate (91). Consumption of inorganic nitrate can itself cause alterations to the oral microbiome (92). Furthermore, both aging (93, 94) and consumption of a sugar-rich diet (95) are known to alter the composition of the oral microbiota, and changes in the oral microbiome have also been identified in individuals with obesity, reflective of concomitant changes in the gastrointestinal tract (96). Specifically, sugar-rich diets can result in a facultative shift in the oral flora toward saccharolytic, acidogenic, and aciduric species (95), and aging is associated with decreased species diversity and increased numbers of opportunistic pathogens (93). Given that specific species of Streptococcus, Staphylococcus, Nocardia, and Corynebacterium are key for nitrate reduction (97, 98), an interesting avenue for future research would be to investigate whether those species are maintained during prolonged HFHS feeding and aging.

Additionally, our finding of increased cardiac fibrosis in HFHS-NO₃ mice contrasts with previous studies that have shown a nitrate-driven amelioration of fibrosis in the kidney and heart as a result of obesity or hypertension in rodent models (99-102). This apparent discrepancy may be attributable to the significantly longer timescale investigated here, compared with a maximum of 10 wk in previous studies. Alternatively, an endothelial-to-mesenchymal transition due to inflammation or a perturbation in redox homeostasis, along with the known reduced effectiveness of the Nrf2 system (and thus fibrosis resolution) with aging (103, 104), may account for the increased cardiac fibrosis seen here. This elevation in cardiac fibrosis was particularly surprising to find in HFHS-NO₃ mice, given the anti-inflammatory effects purported for nitro-fatty acids (nitro-FAs): endogenously produced electrophilic metabolites resulting from the nonenzymatic reaction between unsaturated fatty acids and NO/NO₂⁻ oxidation products (105, 106). Whereas the HFHS diet given to these mice was predominantly high in saturated fats, the unsaturated fat content was thrice that of the standard laboratory chow [6.6% vs. 2.2% (wt/wt), according to manufacturer analyses], which would be suspected to result in increased nitro-FAs concomitantly. However, as the antiinflammatory effects of nitro-FAs occur, at least partially, through activation of the Nrf2 system (106, 107), perhaps the age-related decline in effectiveness also accounts for the surprising increase in fibrosis. If not, there may perhaps be an alteration of the balance of nitro-FA formation and the relationship with Nrf2-mediated processes that leads to an

Figure 4. Inorganic nitrate supplementation offers minor benefits to cardiac fat metabolism in high-fat, high-sucrose (HFHS)-fed mice but worsens cardiac fibrosis. A: total cardiac triacylglycerol (TAG) content, determined by liquid chromatography-mass spectrometry (LC-MS), measured as total peak area ratio normalized to an appropriate internal standard and sample protein concentration. B: total cardiac diacylglycerol (DAG) content, determined by LC-MS, measured as total peak area ratio normalized to an appropriate internal standard and sample protein concentration. C: relative levels of free (no associated acyl chain), short-chain (C2–C5), medium-chain (C6–C12), and long-chain (≥C13) acyl-carnitines to the total carnitine pool as measured by LC-MS from cardiac tissue. D: relative levels of medium-chain acyl-carnitines to the total carnitine pool (from H) shown as an expanded inset. E: contribution of the F pathway via β-oxidation to maximal oxidative phosphorylation (OXPHOS) (FCR_F) in saponin-permeabilized cardiac fibers. F: capacity for OXPHOS supported by octanoyl-carnitine and malate relative to pyruvate and malate (FCR_{FA/P}) in saponin-permeabilized cardiac fibers. G: representative cardiac midsections stained with picrosirius red (PSR) at ×10 magnification. Scale bars, 250 μm. Collagen fibers are stained red, identifying regions of fibrosis. H: quantification of area staining position for PSR, as an indicator of cardiac fibrosis. Data represent means \pm SE; N=6-8 mice/group. *P<0.05, **P<0.01, ***P<0.01, *** ****P < 0.0001, 2-way ANOVA with Tukey's post hoc honestly significant difference (HSD) test for multiple comparisons.

unfavorable shift in the wrong direction in HFHS-NO₃-fed mice. In future work, it would also be interesting to examine the impact of combined long-term HFHS feeding with NO₃⁻ supplementation on vascular function and blood pressure, considering the elevated fibrosis elucidated here. Although not examined in the present study, the well-known hypotensive effects of NO (108, 109), which have been observed to be achievable via dietary inorganic nitrate (110-112), are likely to



interact with the hypertensive effects of a HFHS diet (8, 113, 114), warranting further investigation into nitrate-based approaches to treat hypertension over longer timescales against the background of obesogenic diets.

An unexpected finding in this study was the increased incidence of liver tumors in 12-mo HFHS-NO₃-fed mice, with gene expression analysis suggesting that concurrent HFHS-NO₃ feeding accelerated progression from MASLD to HCC. The pathogenesis of MASLD-associated HCC is incompletely understood, as, despite MASLD being the most common underlying risk factor for HCC (115), only a minority of MASLD patients go on to develop HCC (116). The current hypothesized factors underlying the increased HCC risk in MASLD include compensatory hyperproliferation to counter hepatocyte cell death (as a result of lipotoxicity or DNA damage from oxidative damage), activation of hepatic stellate cells resulting in increased fibrosis, and elevated inflammatory factors (116). Although inorganic nitrate was administered to mice at a low dose, it was expected to increase NO bioavailability, which, while not considered to be damaging to DNA alone, can produce reactive nitrogen species (RNS) upon reacting with reactive oxygen species (ROS) that can damage DNA through both base mutations and strand breaks (117). MASLD has been associated with increased ROS production as a result of fatty acid overload, which may reduce mitochondrial coupling and increase inner mitochondrial membrane electron leak (118). The combined increase of ROS (as a result of the HFHS diet) and NO (as a result of dietary nitrate) may therefore be a key event precipitating the increased incidence of apparent HCC with HFHS-NO₃ feeding. Although the reduction of nitrate to nitrite is likely slow and quantitatively moderate, tissue nitrite may exceed levels in the circulation (88); thus we cannot exclude the possibility that liver tumors may be induced as a result of enhanced nitrosamine formation. The high hepatic concentration of key reductive enzymes, such as xanthine oxidoreductase and (under hypoxic conditions) cytochrome P-450 enzymes (119-121), although not measured in our study, may also facilitate an elevated level of RNS in cases of HFHS-NO₃ feeding, thus contributing to the unexpected malignancies observed here. However, the exact products and posttranslational modifications formed and the subsequent reactions leading to oncogenesis remain unknown and warrant further investigation.

It is unlikely that nitrite/NO-adducts themselves are directly causing the increased malignancy; instead, our results are more likely to reflect the outcome of a complex systems response to changes triggered by the obesogenic diet and

chronic nitrate supplementation administered concomitantly. For instance, pathogenic extracellular matrix (ECM) remodeling has been shown to occur in both the brain (122) and skeletal muscle (123) after obesogenic diets and thus is likely to occur in all metabolically active tissues. Such ECM-driven alterations will lead to inflammation, which will alter the local redox landscape within which cells communicate, which, in turn, will affect DNA repair processes and may possibly increase the propensity for malignancy. The combined effect of nitrate supplementation may escalate these redox changes by, for instance, altering cellular pH (124) and thus elevate this malignancy risk further. Whether such an mechanism is indeed at play here would be an interesting avenue for future research.

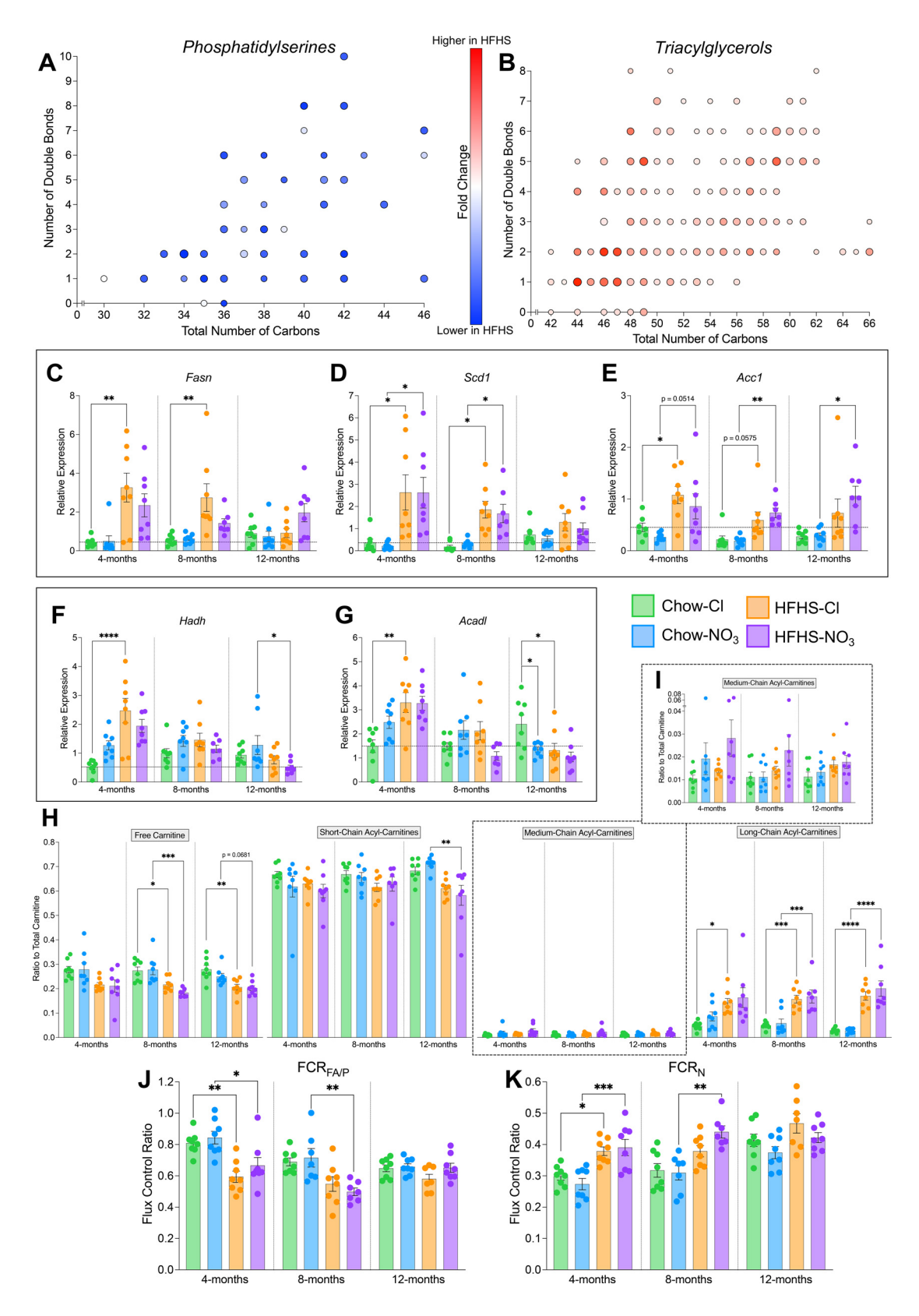
Several studies have highlighted the potential benefits of nitrate supplementation in obesity-related metabolic diseases (28, 31–33, 125). Much of this work stems from the initial observation that dietary inorganic nitrate increased NO bioavailability, offsetting the fall in endogenous NO production, which may be a key pathological event in the development of MetS (28). However, these experiments were carried out on eNOS-deficient mice (28), raising the possibility that nitrate may only be beneficial against the background of reduced endogenous NO production. Inorganic nitrate supplementation may be less effective in cases of MetS or T2DM, where endogenous NOS enzymes are functional, as, although there can be impaired eNOS activity in MetS and T2DM (126, 127), there is a more subtle endogenous NO depletion than that seen in eNOS-deficient mice. Support for this arises from the observation that 12-wk nitrate supplementation did not ameliorate MetS development in high-fat diet-fed mice (128), much as nitrate supplementation did not improve adiposity or HOMA-IR in the HFHS-fed mice in this study.

Despite these negative findings, nitrate may yet hold benefit as a therapeutic agent in certain individuals with obesity-related metabolic disease. eNOS polymorphisms have been associated with T2DM and MetS (14, 15), highlighting a group of patients in which nitrate supplementation may prove to be a beneficial treatment strategy. Furthermore, a higher intake of leafy green vegetables (the largest dietary source of inorganic nitrate) (129) is associated with a 14% reduced risk of T2DM development (130). Although this may be a result of general dietary habits (i.e., individuals who consume more leafy vegetables may consume less processed foods), it highlights the possibility of a preventative role of nitrate in T2DM development as opposed to using it as a therapeutic agent for the treatment of the condition.

Nevertheless, our work highlights that nitrate supplementation is largely ineffective in protecting against the significant

Figure 5. Inorganic nitrate supplementation accelerates the severity of metabolic dysfunction-associated steatotic liver disease (MASLD) in mice. A: liver mass, normalized to total body mass, in 12-mo-old mice. B: prevalence of tumors, visible with the naked eye, in livers from 12-mo-old mice. C: relative hepatic expression of Akr1b10, a marker known to positively associate with hepatocellular carcinoma (HCC) progression, determined by RT-qPCR. D: relative hepatic expression of Spp1, a marker known to positively associate with HCC progression, determined by RT-qPCR. E: relative hepatic expression of Hrg, a marker known to negatively associate with HCC progression, determined by RT-qPCR. F: representative liver sections stained with hematoxylin and eosin (H&E) at ×20 magnification. Scale bars, 150 µm. Arrows highlight examples of hepatocyte ballooning; arrowheads highlight examples of immune invasion foci. HFHS, high-fat, high-sucrose diet. G: representative liver sections stained with oil red O (ORO) at ×20 magnification. Scale bars, 150 μm. Neutral lipids and triglycerides are stained red. H: representative liver sections stained with picrosirius red (PSR) at ×10 magnification. Scale bars, 250 µm. Collagen fibers are stained red, identifying regions of fibrosis. I: MASLD activity score (MAS) determined from blinded histological scoring (Supplemental Table S2). J: hepatic lipid content determined by modified Folch extraction of lipids. K: relative hepatic expression of Serpine1, a marker of fibrosis, determined by RT-qPCR. L: relative hepatic expression of Pdgfb, a marker of fibrosis, determined by RT-qPCR. Data represent means ± SE. N=7 or 8 mice/group. * $\dot{P}<0.05$, ** $\dot{P}<0.01$, *** $\dot{P}<0.001$, **** $\dot{P}<0.001$, *** $\dot{P}<0.001$, **** $\dot{P}<0.001$ test for multiple comparisons. For C-E, K, and L, horizontal line indicates relative expression in 4-mo chow/chloride mice.

consequences of long-term HFHS feeding. Furthermore, we have uncovered that negative consequences of nitrate can emerge against the background of an obesogenic diet. Thus, nitrate supplementation is unlikely to be an effective approach to improve metabolic health in obesity, without wider alterations to the diet. Given the recent change in public perception of nitrate as being beneficial rather than detrimental, there is an urgent need to reproduce our findings in other



Combined HFHS+ Nitrate effects

Accelerated MASLD

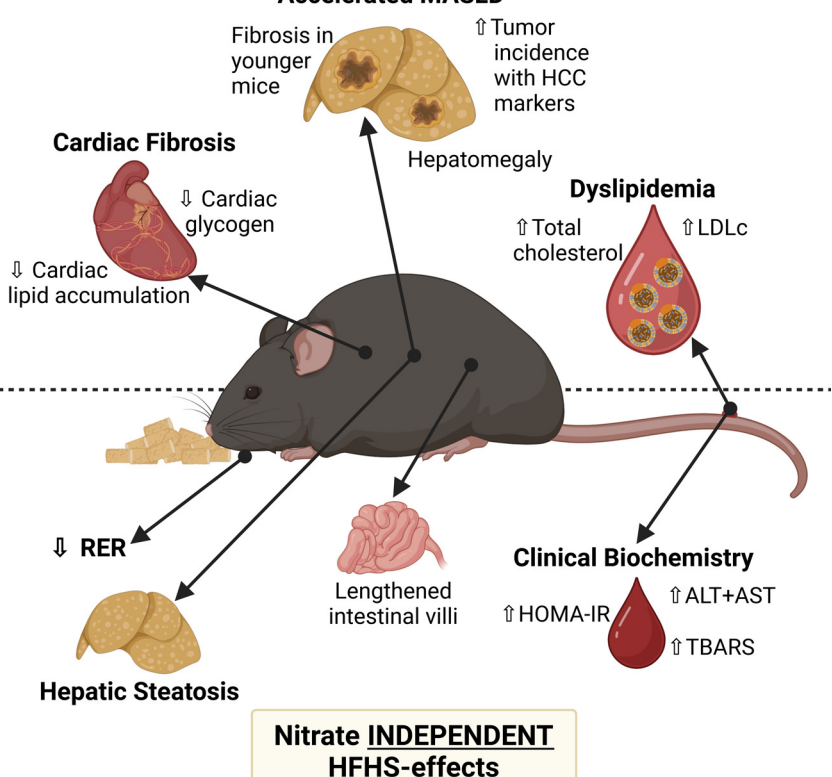


Figure 7. Summary of diet-induced obesity effects determined in this study as a result of high-fat, high-sucrose (HFHS) feeding (independent of nitrate supplementation) or as a result of inorganic nitrate supplementation in combination with HFHS diet. Upward arrow indicates higher in HFHS (compared with chow) or HFHS-NO₃ (compared with HFHS-CI), respectively; downward arrow indicates lower in HFHS (compared with chow) or HFHS-NO₃ (compared with HFHS-CI), respectively. ALT, alanine transaminase; AST, aspartate transaminase; HCC, hepatocellular carcinoma: HOMA-IR, homeostatic model assessment of insulin resistance; LDLc, low-density lipoprotein cholesterol; MASLD, metabolic dysfunctionassociated steatotic liver disease; RER, respiratory exchange ratio; TBARS, thiobarbituric acid reactive substances. Created with BioRender.com.

laboratories and animal models and to investigate the mechanisms of enhanced cardiac fibrosis and hepatic malignancy. This is especially important since epidemiological evidence is emerging that the effects of enhanced nitrate intake on cardiovascular health may be source specific (131).

DATA AVAILABILITY

The datasets supporting the results presented in this article are freely available via the Cambridge University Repository (https://doi. org/10.17863/CAM.112799). Raw metabolomics data are available in the EMBL-EBI MetaboLights database (132) with the study identifier MTBLS9526.

SUPPLEMENTAL MATERIAL

Supplemental Figs. S1-S5 and Supplemental Tables S1 and S2: https://doi.org/10.17863/CAM.112799.

ACKNOWLEDGMENTS

We thank Sarah Royle, Matthew Rodgers, and Mithylan Ganeshwaran for help on the project and Benjamin Stockell for statistical advice. We also thank Hayley Forrest, Alison Robertson, and Ben Jaggs for support with animal work and Joe Lewis for support with the metabolic cage setup. We thank Kat Millen and Sarah Bray for use of thermocycler equipment throughout the study. We thank Hannah Mannering and the Disease Model Core (Wellcome-MRC

Figure 6. High-fat, high-sucrose (HFHS) feeding is associated with remodeling of the hepatic lipidome and rewiring of lipid metabolism in an age-dependent manner. A: hepatic phosphatidylserine (PS) species found to be differentially affected by HFHS feeding in mice [determined by variable importance parameter (VIP) score from partial least square-discriminant analysis (PLS-DA; Supplemental Fig. S4D) > 1], plotted by total number of carbons and double bonds in the acyl chains. B: hepatic triacylglycerol (TAG) species found to be differentially affected by HFHS feeding in mice [VIP score from PLS-DA (Supplemental Fig. S4E) > 1], plotted by total number of carbons and double bonds in the acyl chains. For A and B, size of the point represents the VIP score for the PLS-DA model, and color represents relative fold change in livers from HFHS-fed mice compared to chow-fed mice. C. relative hepatic expression of Fasn, determined by RT-qPCR. Horizontal line indicates relative expression in 4-mo chow/chloride mice. D: relative hepatic expression of Scd1, determined by RT-qPCR. Horizontal line indicates relative expression in 4-mo chow/chloride mice. E: relative hepatic expression of Acc1, determined by RT-qPCR. Horizontal line indicates relative expression in 4-mo chow/chloride mice. F: relative hepatic expression of Hadh, determined by RT-qPCR. Horizontal line indicates relative expression in 4-mo chow/chloride mice. G: relative hepatic expression of Acadl, determined by RT-qPCR. Horizontal line indicates relative expression in 4-mo chow/chloride mice. H: relative levels of free (no associated acyl chain), short-chain (C2-C5), medium-chain (C6-C12), and long-chain (>C13) acyl-carnitines to the total carnitine pool as measured by liquid chromatography-mass spectrometry (LC-MS) from liver tissue. I: relative levels of medium-chain acyl-carnitines to the total carnitine pool (from H) shown as an expanded inset. J: capacity for oxidative phosphorylation (OXPHOS) supported by octanoyl-carnitine and malate relative to pyruvate and malate (FCR_{FA/P}) in liver homogenate. K: contribution of the N pathway via complex I to maximal OXPHOS (FCR_N) in liver homogenate. For C-K, data represent means \pm SE; N=7 or 8 mice/group. *P < 0.05, **P < 0.01, ***P < 0.001, ****P < 0.0001, ****P < 0.0001, ****P < 0.001, ***P < 0.001, **P < 0.001, **2-way ANOVA with Tukey's post hoc honestly significant difference (HSD) test for multiple comparisons.



Institute of Metabolic Sciences) for technical assistance in DEXA scans, James Warner and the Histopathology Core [MRC Metabolic Diseases Unit (MC_UU_00014/5)] for processing and embedding liver samples, and Peter Barker, Keith Burling, and the Cambridge Biochemical Assay Laboratory (Cambridge University Hospitals NHS Foundation Trust) for clinical chemistry analyses.

Present addresses: A. P. Sowton, Medical Research Council Mitochondrial Biology Unit, University of Cambridge, Cambridge, CB2 OXY, United Kingdom; R. Baxter, Dept. of Pharmacology, University of Cambridge, Cambridge, CB2 1PD, United Kingdom; G. Mocciaro, Roger Williams Institute of Hepatology, Foundation for Liver Research, London, SE5 9NT, United Kingdom; M. Vacca, Dept. of Interdisciplinary Medicine, Clinica Medica "C. Frugoni," Aldo Moro University of Bari, 70124 Bari, Italy.

Graphical Abstract created with BioRender.com.

For the purpose of open access, the author has applied a Creative Commons Attribution (CC BY) license to any Author Accepted Manuscript version arising from this submission.

GRANTS

This work was supported by 4-yr PhD studentships from the British Heart Foundation, Grant Numbers FS/17/61/33473 (to A.P.S.). FS/4yPhD/F/21/34156 (to R.B.), FS/18/56/34177 (to D.K.K.), and FS/ 4yPhD/F/20/34124 (to B.D.T.); Rank Prize Fund Nutrition Covid Response Grant (to A.P.S.); 4-yr PhD studentship from the Wellcome Trust, Grant Number 220033/Z/19/Z (to L.M.W.H.); Biotechnology and Biological Sciences Research Council Doctoral Training Program, Grant Number BB/M011194/1 (to P.M.D.); Medical Research Council Lipid Profiling and Signalling & Lipid Dynamics and Regulation, Grants Numbers MC UP A90 1006 and MC PC 13030 (to G.M., M.V., and J.L.G.); Research Councils UK, Grant Number EP/E500552/1 (to A.J.M.); and Evelyn Trust, Grant Number 16/33 (to A.J.M.).

DISCLOSURES

No conflicts of interest, financial or otherwise, are declared by the authors.

AUTHOR CONTRIBUTIONS

A.P.S., M.V., M.F., J.L.G., and A.J.M. conceived and designed research; A.P.S., L.M.W.H., F.N.K., R.B., G.M., D.K.K., M.M., K.A.O., M.C.H., P.M.D., and B.D.T. performed experiments; A.P.S. analyzed data; A.P.S. interpreted results of experiments; A.P.S. prepared figures; A.P.S. drafted manuscript; A.P.S., M.F., J.L.G., and A.J.M. edited and revised manuscript; A.P.S., L.M.W.H., F.N.K., R.B., G.M., D.K.K., M.M., K.A.O., M.C.H., P.M.D., B.D.T., M.V., M.F., J.L.G., and A.J.M. approved final version of manuscript.

REFERENCES

- Afshin A, Forouzanfar MH, Reitsma MB, Sur P, Estep K, Lee A; et al. Health effects of overweight and obesity in 195 countries over 25 years. N Engl J Med 377: 13-27, 2017. doi:10.1056/NEJMoa1614362.
- Global BMI Mortality Collaboration, Di Angelantonio E, Bhupathiraju S, Wormser D, Gao P, Kaptoge S, Berrington de Gonzalez A, et al. Body-mass index and all-cause mortality: individual-participant-data meta-analysis of 239 prospective studies in four continents. Lancet 388: 776-786, 2016. doi:10.1016/S0140-6736(16)30175-1.
- Engin A. The definition and prevalence of obesity and metabolic syndrome. Adv Exp Med Biol 960: 1-17, 2017. doi:10.1007/978-3-319-
- Wang YC, McPherson K, Marsh T, Gortmaker SL, Brown M. Health and economic burden of the projected obesity trends in the USA and the UK. Lancet 378: 815-825, 2011 [Erratum in Lancet 378: 1778, 2011]. doi:10.1016/S0140-6736(11)60814-3.

- Kahn SE, Hull RL, Utzschneider KM. Mechanisms linking obesity to insulin resistance and type 2 diabetes. Nature 444: 840-846, 2006. doi:10.1038/nature05482.
- Kim MS, Kim WJ, Khera AV, Kim JY, Yon DK, Lee SW, Shin JI, Won HH. Association between adiposity and cardiovascular outcomes: an umbrella review and meta-analysis of observational and Mendelian randomization studies. Eur Heart J 42: 3388–3403, 2021. doi:10.1093/eurheartj/ehab454.
- Milić S, Lulić D, Štimac D. Non-alcoholic fatty liver disease and obesity: biochemical, metabolic and clinical presentations. World J Gastroenterol 20: 9330-9337, 2014. doi:10.3748/wjg.v20.i28.9330.
- Weidmann P, Boehlen LM, de Courten M. Pathogenesis and treatment of hypertension associated with diabetes mellitus. Am Heart J 125: 1498-1513, 1993, doi:10.1016/0002-8703(93)90447-h.
- 9. Huang PL, Huang Z, Mashimo H, Bloch KD, Moskowitz MA, Bevan JA, Fishman MC. Hypertension in mice lacking the gene for endothelial nitric oxide synthase. Nature 377: 239-242, 1995. doi:10.1038/ 377239a0
- Duplain H, Burcelin R, Sartori C, Cook S, Egli M, Lepori M, Vollenweider P, Pedrazzini T, Nicod P, Thorens B, Scherrer U. Insulin resistance, hyperlipidemia, and hypertension in mice lacking endothelial nitric oxide synthase. Circulation 104: 342-345, 2001. doi:10.1161/01.cir.104.3.342.
- Cook S, Hugli O, Egli M, Vollenweider P, Burcelin R, Nicod P, Thorens B, Scherrer U. Clustering of cardiovascular risk factors mimicking the human metabolic syndrome X in eNOS null mice. Swiss Med Wkly 133: 360-363, 2003. doi:10.4414/smw.2003.10239.
- Nisoli E, Clementi E, Paolucci C, Cozzi V, Tonello C, Sciorati C, Bracale R, Valerio A, Francolini M, Moncada S, Carruba MO. Mitochondrial biogenesis in mammals: the role of endogenous nitric oxide. Science 299: 896-899, 2003. doi:10.1126/science.1079368.
- Le Gouill E, Jimenez M, Binnert C, Jayet PY, Thalmann S, Nicod P, Scherrer U, Vollenweider P. Endothelial nitric oxide synthase (eNOS) knockout mice have defective mitochondrial β -oxidation. Diabetes 56: 2690-2696, 2007. doi:10.2337/db06-1228.
- Monti LD, Barlassina C, Citterio L, Galluccio E, Berzuini C, Setola E, Valsecchi G, Lucotti P, Pozza G, Bernardinelli L, Casari G, Piatti P. Endothelial nitric oxide synthase polymorphisms are associated with type 2 diabetes and the insulin resistance syndrome. Diabetes 52: 1270-1275, 2003. doi:10.2337/diabetes.52.5.1270.
- Fernandez ML, Ruiz R, Gonzalez MA, Ramirez-Lorca R, Couto C, Ramos A, Gutierrez-Tous R, Rivera JM, Ruiz A, Real LM, Grilo A. Association of NOS3 gene with metabolic syndrome in hypertensive patients. Thromb Haemost 92: 413-418, 2004. doi:10.1160/TH04-02-
- Avogaro A, Toffolo G, Kiwanuka E, de Kreutzenberg SV, Tessari P, Cobelli C. L-arginine-nitric oxide kinetics in normal and type 2 diabetic subjects: a stable-labelled ¹⁵N arginine approach. *Diabetes* 52: 795-802, 2003. doi:10.2337/diabetes.52.3.795.
- Lundberg JO, Govoni M. Inorganic nitrate is a possible source for systemic generation of nitric oxide. Free Radic Biol Med 37: 395-400, 2004. doi:10.1016/j.freeradbiomed.2004.04.027.
- Duncan C, Dougall H, Johnston P, Green S, Brogan R, Leifert C, Smith L, Golden M, Benjamin N. Chemical generation of nitric oxide in the mouth from the enterosalivary circulation of dietary nitrate. Nat Med 1: 546-551, 1995. doi:10.1038/nm0695-546.
- Lundberg JO, Weitzberg E, Lundberg JM, Alving K. Intragastric nitric oxide production in humans: measurements in expelled air. Gut 35: 1543-1546, 1994. doi:10.1136/gut.35.11.1543.
- Lundberg JO, Weitzberg E, Gladwin MT. The nitrate-nitrite-nitric oxide pathway in physiology and therapeutics. Nat Rev Drug Discov 7: 156-167, 2008. doi:10.1038/nrd2466.
- 21. Zhang Z, Naughton DP, Blake DR, Benjamin N, Stevens CR, Winyard PG, Symons MC, Harrison R. Human xanthine oxidase converts nitrite ions into nitric oxide (NO). Biochem Soc Trans 25: 524S, 1997. doi:10.1042/bst025524s.
- 22. Cosby K, Partovi KS, Crawford JH, Patel RP, Reiter CD, Martyr S, Yang BK, Waclawiw MA, Zalos G, Xu X, Huang KT, Shields H, Kim-Shapiro DB, Schechter AN, Cannon RO 3rd, Gladwin MT. Nitrite reduction to nitric oxide by deoxyhemoglobin vasodilates the human circulation. Nat Med 9: 1498-1505, 2003. doi:10.1038/nm954.
- 23. Shiva S, Huang Z, MacArthur PH, Ringwood LA, Gladwin MT. Myoglobin is a nitrite reductase that generates NO and regulates

- mitochondrial respiration (Abstract). Blood 108: 1561, 2006. doi:10.1182/blood.V108.11.1561.1561.
- 24. Moncada S, Higgs A. The L-arginine-nitric oxide pathway. N Engl J Med 329: 2002-2012, 1993. doi:10.1056/NEJM199312303292706.
- 25. Sindelar JJ, Milkowski AL. Human safety controversies surrounding nitrate and nitrite in the diet. Nitric Oxide 26: 259-266, 2012. doi:10.1016/ i niox 2012 03 011.
- 26. Zweier JL, Wang P, Samouilov A, Kuppusamy P. Enzyme-independent formation of nitric oxide in biological tissues. Nat Med 1: 804-809, 1995. doi:10.1038/nm0895-804.
- 27. Butler AR, Feelisch M. Therapeutic uses of inorganic nitrite and nitrate: from the past to the future. Circulation 117: 2151-2159, 2008. doi:10.1161/CIRCULATIONAHA.107.753814.
- 28. Carlström M, Larsen FJ, Nyström T, Hezel M, Borniquel S, Weitzberg E, Lundberg JO. Dietary inorganic nitrate reverses features of metabolic syndrome in endothelial nitric oxide synthase-deficient mice. Proc Natl Acad Sci USA 107: 17716-17720, 2010. doi:10.1073/pnas. 1008872107
- 29. Jiang H, Torregrossa AC, Potts A, Pierini D, Aranke M, Garg HK, Bryan NS. Dietary nitrite improves insulin signaling through GLUT4 translocation. Free Radic Biol Med 67: 51-57, 2014. doi:10.1016/j. freeradbiomed.2013.10.809.
- Singamsetty S, Watanabe Y, Guo L, Corey C, Wang Y, Tejero J, McVerry BJ, Gladwin MT, Shiva S, O'Donnell CP. Inorganic nitrite improves components of the metabolic syndrome independent of weight change in a murine model of obesity and insulin resistance. J Physiol 593: 3135-3145, 2015. doi:10.1113/JP270386.
- 31. Essawy SS, Abdel-Sater KA, Elbaz AA. Comparing the effects of inorganic nitrate and allopurinol in renovascular complications of metabolic syndrome in rats: role of nitric oxide and uric acid. Arch Med Sci 10: 537-545, 2014. doi:10.5114/aoms.2013.33222.
- Gheibi S, Jeddi S, Carlström M, Gholami H, Ghasemi A. Effects of long-term nitrate supplementation on carbohydrate metabolism, lipid profiles, oxidative stress, and inflammation in male obese type 2 diabetic rats. Nitric Oxide 75: 27-41, 2018. doi:10.1016/j.niox.2018.02.002.
- 33. Li T, Lu X, Sun Y, Yang X. Effects of spinach nitrate on insulin resistance, endothelial dysfunction markers and inflammation in mice with high-fat and high-fructose consumption. Food Nutr Res 60: 32010, 2016. doi:10.3402/fnr.v60.32010.
- Ashmore T, Fernandez BO, Branco-Price C, West JA, Cowburn AS, Heather LC, Griffin JL, Johnson RS, Feelisch M, Murray AJ. Dietary nitrate increases arginine availability and protects mitochondrial complex I and energetics in the hypoxic rat heart. J Physiol 592: 4715-4731, 2014. doi:10.1113/jphysiol.2014.275263.
- 35. Ashmore T, Roberts LD, Morash AJ, Kotwica AO, Finnerty J, West JA, Murfitt SA, Fernandez BO, Branco C, Cowburn AS, Clarke K, Johnson RS, Feelisch M, Griffin JL, Murray AJ. Nitrate enhances skeletal muscle fatty acid oxidation via a nitric oxide-cGMP-PPARmediated mechanism. BMC Biol 13: 110, 2015. doi:10.1186/s12915-015-0221-6.
- Horscroft JA, O'Brien KA, Clark AD, Lindsay RT, Steel AS, Procter NE, Devaux J, Frenneaux M, Harridge SD, Murray AJ. Inorganic nitrate, hypoxia, and the regulation of cardiac mitochondrial respiration-probing the role of PPARa. FASEB J 33: 7563-7577, 2019. doi:10.1096/fj.201900067R.
- 37. Ivarsson N, Schiffer TA, Hernández A, Lanner JT, Weitzberg E, Lundberg JO, Westerblad H. Dietary nitrate markedly improves voluntary running in mice. Physiol Behav 168: 55-61, 2017. doi:10.1016/j. physbeh.2016.10.018.
- 38. Roberts LD, Ashmore T, Kotwica AO, Murfitt SA, Fernandez BO, Feelisch M, Murray AJ, Griffin JL. Inorganic nitrate promotes the browning of white adipose tissue through the nitrate-nitrite-nitric oxide pathway. Diabetes 64: 471-484, 2015. doi:10.2337/db14-0496.
- Peleli M, Ferreira DM, Tarnawski L, McCann Haworth S, Xuechen L, Zhuge Z, Newton PT, Massart J, Chagin AS, Olofsson PS, Ruas JL, Weitzberg E, Lundberg JO, Carlström M. Dietary nitrate attenuates high-fat diet-induced obesity via mechanisms involving higher adipocyte respiration and alterations in inflammatory status. Redox Biol 28: 101387, 2020. doi:10.1016/j.redox.2019.101387.
- McNally BD, Moran A, Watt NT, Ashmore T, Whitehead A, Murfitt SA, Kearney MT, Cubbon RM, Murray AJ, Griffin JL, Roberts LD. Inorganic nitrate promotes glucose uptake and oxidative catabolism in white adipose tissue through the XOR-catalyzed nitric oxide pathway. Diabetes 69: 893-901, 2020. doi:10.2337/db19-0892.

- 41. Tateya S, Rizzo NO, Handa P, Cheng AM, Morgan-Stevenson V, Daum G, Clowes AW, Morton GJ, Schwartz MW, Kim F. Endothelial NO/cGMP/VASP signaling attenuates Kupffer cell activation and hepatic insulin resistance induced by high-fat feeding. Diabetes 60: 2792-2801, 2011. doi:10.2337/db11-0255.
- 42. Hezel MP, Liu M, Schiffer TA, Larsen FJ, Checa A, Wheelock CE, Carlström M, Lundberg JO, Weitzberg E. Effects of long-term dietary nitrate supplementation in mice. Redox Biol 5: 234-242, 2015. doi:10.1016/j.redox.2015.05.004.
- Matthews DR, Hosker JP, Rudenski AS, Naylor BA, Treacher DF, Turner RC. Homeostasis model assessment: insulin resistance and β-cell function from fasting plasma glucose and insulin concentrations in man. Diabetologia 28: 412–419, 1985. doi:10.1007/BF00280883.
- 44. Hippisley-Cox J, Coupland C, Brindle P. Development and validation of QRISK3 risk prediction algorithms to estimate future risk of cardiovascular disease: prospective cohort study. BMJ 357: j2099, 2017. doi:10.1136/bmj.j2099.
- Taylor SR, Ramsamooj S, Liang RJ, Katti A, Pozovskiy R, Vasan N, Hwang SK, Nahiyaan N, Francoeur NJ, Schatoff EM, Johnson JL, Shah MA, Dannenberg AJ, Sebra RP, Dow LE, Cantley LC, Rhee KY, Goncalves MD. Dietary fructose improves intestinal cell survival and nutrient absorption. Nature 597: 263-267, 2021. doi:10.1038/ s41586-021-03827-2.
- 46. Weir JB. New methods for calculating metabolic rate with special reference to protein metabolism. J Physiol 109: 1-9, 1949. doi:10.1113/ jphysiol.1949.sp004363.
- 47. Virtue S, Lelliott CJ, Vidal-Puig A. What is the most appropriate covariate in ANCOVA when analysing metabolic rate? Nat Metab 3: 1585, 2021. doi:10.1038/s42255-021-00505-5.
- 48. Mina Al, LeClair RA, LeClair KB, Cohen DE, Lantier L, Banks AS. CalR: a web-based analysis tool for indirect calorimetry experiments. Cell Metab 28: 656-666.e1, 2018. doi:10.1016/j.cmet.2018.06.019.
- 49. R Core Team. R: A language and environment for statistical computing (Online).R Foundation for Statistical Computing. https:// www.r-project.org/.
- 50. Friedewald WT, Levy RI, Fredrickson DS. Estimation of concentration of low-density lipoprotein cholesterol in plasma, without use of preparative ultracentrifuge. Clin Chem 18: 499-502, 1972.
- van Dijk TH, Laskewitz AJ, Grefhorst A, Boer TS, Bloks VW, Kuipers F, Groen AK, Reijngoud DJ. A novel approach to monitor glucose metabolism using stable isotopically labelled glucose in longitudinal studies in mice. Lab Anim 47: 79-88, 2013. doi:10.1177/ 0023677212473714.
- 52. Mencke R, Al Ali L, de Koning ML, Pasch A, Minnion M, Feelisch M, van Veldhuisen DJ, van der Horst IC, Gansevoort RT, Bakker SJ, de Borst MH, van Goor H, van der Harst P, Lipsic E, Hillebrands JL. Serum calcification propensity is increased in myocardial infarction and hints at a pathophysiological role independent of classical cardiovascular risk factors. Arterioscler Thromb Vasc Biol 44: 1884–1894, 2024. doi:10.1161/ATVBAHA.124.320974.
- McKenna HT, O'Brien KA, Fernandez BO, Minnion M, Tod A, McNally BD, West JA, Griffin JL, Grocott MP, Mythen MG, Feelisch M, Murray AJ, Martin DS. Divergent trajectories of cellular bioenergetics, intermediary metabolism and systemic redox status in survivors and non-survivors of critical illness. Redox Biol 41: 101907, 2021. doi:10.1016/j.redox.2021.101907.
- 54. Bialkowska AB, Ghaleb AM, Nandan MO, Yang VW. Improved Swiss-rolling technique for intestinal tissue preparation for immunohistochemical and immunofluorescent analyses. J Vis Exp 113: e54161, 2016. doi:10.3791/54161.
- 55. Mopuri R, Kalyesubula M, Rosov A, Edery N, Moallem U, Dvir H. Improved Folch method for liver-fat quantification. Front Vet Sci 7: 594853, 2020. doi:10.3389/fvets.2020.594853.
- Horscroft JA, Burgess SL, Hu Y, Murray AJ. Altered oxygen utilisation in rat left ventricle and soleus after 14 days, but not 2 days, of environmental hypoxia. PLoS One 10: e0138564, 2015. doi:10.1371/ journal.pone.0138564.
- 57. Sowton AP, Padmanabhan N, Tunster SJ, McNally BD, Murgia A, Yusuf A, Griffin JL, Murray AJ, Watson ED. Mtrr hypomorphic mutation alters liver morphology, metabolism and fuel storage in mice. Mol Genet Metab Rep 23: 100580, 2020. doi:10.1016/j.ymgmr. 2020.100580.
- 58. Bligh EG, Dyer WJ. A rapid method of total lipid extraction and purification. Can J Biochem Physiol 37: 911-917, 1959. doi:10.1139/o59-099.

- 59. McNally BD, Ashley DF, Hänschke L, Daou HN, Watt NT, Murfitt SA, MacCannell AD, Whitehead A, Bowen TS, Sanders FW, Vacca M, Witte KK, Davies GR, Bauer R, Griffin JL, Roberts LD. Long-chain ceramides are cell non-autonomous signals linking lipotoxicity to endoplasmic reticulum stress in skeletal muscle. Nat Commun 13: 1748, 2022. doi:10.1038/s41467-022-29363-9.
- 60. Hall Z, Chiarugi D, Charidemou E, Leslie J, Scott E, Pellegrinet L, Allison M, Mocciaro G, Anstee QM, Evan GI, Hoare M, Vidal-Puig A, Oakley F, Vacca M, Griffin JL. Lipid remodeling in hepatocyte proliferation and hepatocellular carcinoma. Hepatology 73: 1028-1044, 2021. doi:10.1002/hep.31391.
- 61. Smith CA, Want EJ, O'Maille G, Abagyan R, Siuzdak G. XCMS: processing mass spectrometry data for metabolite profiling using nonlinear peak alignment, matching, and identification. Anal Chem 78: 779-787, 2006. doi:10.1021/ac051437y.
- 62. Sud M, Fahy E, Cotter D, Brown A, Dennis EA, Glass CK, Merrill AH Jr, Murphy RC, Raetz CR, Russell DW, Subramaniam S. LMSD: LIPID MAPS structure database. Nucleic Acids Res 35: D527–D532, 2007. doi:10.1093/nar/gkl838.
- 63. Kleiner DE, Brunt EM, Van Natta M, Behling C, Contos MJ, Cummings OW, Ferrell LD, Liu YC, Torbenson MS, Unalp-Arida A, Yeh M, McCullough AJ, Sanyal AJ; Nonalcoholic Steatohepatitis Clinical Research Network. Design and validation of a histological scoring system for nonalcoholic fatty liver disease. Hepatology 41: 1313-1321, 2005. doi:10.1002/hep.20701.
- 64. Schindelin J, Arganda-Carreras I, Frise E, Kaynig V, Longair M, Pietzsch T, Preibisch S, Rueden C, Saalfeld S, Schmid B, Tinevez JY, White DJ, Hartenstein V, Eliceiri K, Tomancak P, Cardona A. Fiji: an open-source platform for biological-image analysis. Nat Methods 9: 676-682, 2012. doi:10.1038/nmeth.2019.
- 65. Pratt DS, Kaplan MM. Evaluation of abnormal liver-enzyme results in asymptomatic patients. N Engl J Med 342: 1266-1271, 2000. doi:10.1056/NEJM200004273421707.
- 66. Larsen FJ, Schiffer TA, Borniquel S, Sahlin K, Ekblom B, Lundberg JO, Weitzberg E. Dietary inorganic nitrate improves mitochondrial efficiency in humans. Cell Metab 13: 149-159, 2011. doi:10.1016/j. cmet.2011.01.004.
- 67. Assaad H, Yao K, Tekwe CD, Feng S, Bazer FW, Zhou L, Carroll RJ, Meininger CJ, Wu G. Analysis of energy expenditure in diet-induced obese rats. Front Biosci (Landmark Ed) 19: 967-985, 2014. doi:10.2741/4261.
- 68. Simonson DC, DeFronzo RA. Indirect calorimetry: methodological and interpretative problems. Am J Physiol Endocrinol Metab 258: E399-E412, 1990. doi:10.1152/ajpendo.1990.258.3.E399.
- 69. Stump CS, Henriksen EJ, Wei Y, Sowers JR. The metabolic syndrome: role of skeletal muscle metabolism. Ann Med 38: 389-402, 2006. doi:10.1080/07853890600888413.
- 70. Jansson E. On the significance of the respiratory exchange ratio after different diets during exercise in man. Acta Physiol Scand 114: 103-110, 1982. doi:10.1111/j.1748-1716.1982.tb06958.x.
- Burkholder TJ, Fingado B, Baron S, Lieber RL. Relationship between muscle fiber types and sizes and muscle architectural properties in the mouse hindlimb. J Morphol 221: 177-190, 1994. doi:10.1002/jmor.1052210207.
- Pappachan JM, Varughese GI, Sriraman R, Arunagirinathan G. Diabetic cardiomyopathy: Pathophysiology, diagnostic evaluation and management. World J Diabetes 4: 177-189, 2013. doi:10.4239/wjd.v4. i5 177
- 73. Bugger H, Abel ED. Molecular mechanisms of diabetic cardiomyopathy. Diabetologia 57: 660-671, 2014. doi:10.1007/s00125-014-3171-6.
- 74. Yin FC, Spurgeon HA, Rakusan K, Weisfeldt ML, Lakatta EG. Use of tibial length to quantify cardiac hypertrophy: application in the aging rat. Am J Physiol Heart Circ Physiol 243: H941-H947, 1982. doi:10.1152/ajpheart.1982.243.6.H941.
- 75. Warren S. The effect of insulin on pathologic glycogen deposits in diabetes mellitus. Am J Med Sci 179: 482-488, 1930. doi:10.1097/ 00000441-193004000-00003.
- 76. Reichelt ME, Mellor KM, Curl CL, Stapleton D, Delbridge LM. Myocardial glycophagy—a specific glycogen handling response to metabolic stress is accentuated in the female heart. J Mol Cell Cardiol 65: 67-75, 2013. doi:10.1016/j.yjmcc.2013.09.014.
- 77. Lopaschuk GD, Ussher JR, Folmes CD, Jaswal JS, Stanley WC. Myocardial fatty acid metabolism in health and disease. Physiol Rev 90: 207-258, 2010. doi:10.1152/physrev.00015.2009.

- Neubauer S. The failing heart—an engine out of fuel. N Engl J Med 356: 1140-1151, 2007. doi:10.1056/NEJMra063052.
- Younossi ZM, Koenig AB, Abdelatif D, Fazel Y, Henry L, Wymer M. Global epidemiology of nonalcoholic fatty liver disease—meta-analytic assessment of prevalence, incidence, and outcomes. Hepatology 64: 73-84, 2016. doi:10.1002/hep.28431.
- 80. He X, Wang Y, Zhang W, Li H, Luo R, Zhou Y, Liao CL, Huang H, Lv X, Xie Z, He M. Screening differential expression of serum proteins in AFP-negative HBV-related hepatocellular carcinoma using iTRAQ-MALDI-MS/MS. Neoplasma 61: 17-26, 2014. doi:10.4149/ neo 2014 001.
- Zou X, Zhang D, Song Y, Liu S, Long Q, Yao L, Li W, Duan Z, Wu D, Liu L. HRG switches TNFR1-mediated cell survival to apoptosis in hepatocellular carcinoma. Theranostics 10: 10434-10447, 2020. doi:10.7150/
- Sanders FW, Acharjee A, Walker C, Marney L, Roberts LD, Imamura F, Jenkins B, Case J, Ray S, Virtue S, Vidal-Puig A, Kuh D, Hardy R, Allison M, Forouhi N, Murray AJ, Wareham N, Vacca M, Koulman A, Griffin JL. Hepatic steatosis risk is partly driven by increased de novo lipogenesis following carbohydrate consumption. Genome Biol 19: 79, 2018. doi:10.1186/s13059-018-1439-8.
- 83. McNally B, Griffin JL, Roberts LD. Dietary inorganic nitrate: from villain to hero in metabolic disease? Mol Nutr Food Res 60: 67-78, 2016. doi:10.1002/mnfr.201500153.
- Larsen FJ, Schiffer TA, Ekblom B, Mattsson MP, Checa A, Wheelock CE, Nyström T, Lundberg JO, Weitzberg E. Dietary nitrate reduces resting metabolic rate: a randomized, crossover study in humans. Am J Clin Nutr 99: 843–850, 2014. doi:10.3945/ajcn.113.079491.
- 85. Chiappini F, Coilly A, Kadar H, Gual P, Tran A, Desterke C, Samuel D, Duclos-Vallée JC, Touboul D, Bertrand-Michel J, Brunelle A, Guettier C, Le Naour F. Metabolism dysregulation induces a specific lipid signature of nonalcoholic steatohepatitis in patients. Sci Rep 7: 46658, 2017, doi:10.1038/srep46658,
- 86. Hernández-Alvarez MI, Sebastián D, Vives S, Ivanova S, Bartoccioni P, Kakimoto P, et al. Deficient endoplasmic reticulummitochondrial phosphatidylserine transfer causes liver disease. Cell 177: 881-895.e17, 2019. doi:10.1016/j.cell.2019.04.010.
- Roberts LD, Ashmore T, McNally BD, Murfitt SA, Fernandez BO, Feelisch M, Lindsay R, Siervo M, Williams EA, Murray AJ, Griffin JL. Inorganic nitrate mimics exercise-stimulated muscular fiber-type switching and myokine and γ -aminobutyric acid release. *Diabetes* 66: 674-688, 2017. doi:10.2337/db16-0843.
- Milsom AB, Fernandez BO, Garcia-Saura MF, Rodriguez J, Feelisch M. Contributions of nitric oxide synthases, dietary nitrite/nitrate, and other sources to the formation of NO signaling products. Antioxid Redox Signal 17: 422–432, 2012. doi:10.1089/ars.2011.4156.
- Pannala AS, Mani AR, Spencer JP, Skinner V, Bruckdorfer KR, Moore KP, Rice-Evans CA. The effect of dietary nitrate on salivary, plasma, and urinary nitrate metabolism in humans. Free Radic Biol Med 34: 576-584, 2003. doi:10.1016/s0891-5849(02)01353-9.
- 90. Bryda EC. The Mighty Mouse: the impact of rodents on advances in biomedical research. Mo Med 110: 207-211, 2013.
- Hezel MP, Weitzberg E. The oral microbiome and nitric oxide homoeostasis. Oral Dis 21: 7-16, 2015. doi:10.1111/odi.12157.
- Velmurugan S, Gan JM, Rathod KS, Khambata RS, Ghosh SM, Hartley A, Van Eijl S, Sagi-Kiss V, Chowdhury TA, Curtis M, Kuhnle GG, Wade WG, Ahluwalia A. Dietary nitrate improves vascular function in patients with hypercholesterolemia: a randomized, doubleblind, placebo-controlled study. Am J Clin Nutr 103: 25-38, 2016 [Erratum in Am J Clin Nutr 107: 676, 2018]. doi:10.3945/ajcn.115.116244.
- Zhou X, Wang B, Demkowicz PC, Johnson JS, Chen Y, Spakowicz DJ, Zhou Y, Dorsett Y, Chen L, Sodergren E, Kuchel GA, Weinstock GM. Exploratory studies of oral and fecal microbiome in healthy human aging. Front Aging 3: 1002405, 2022. doi:10.3389/ fragi.2022.1002405.
- Ogawa T, Hirose Y, Honda-Ogawa M, Sugimoto M, Sasaki S, Kibi M, Kawabata S, Ikebe K, Maeda Y. Composition of salivary microbiota in elderly subjects. Sci Rep 8: 414, 2018. doi:10.1038/s41598-017-18677-0
- Rosier BT, Marsh PD, Mira A. Resilience of the oral microbiota in health: mechanisms that prevent dysbiosis. J Dent Res 97: 371–380, 2018. doi:10.1177/0022034517742139.
- 96. Schamarek I, Anders L, Chakaroun RM, Kovacs P, Rohde-Zimmermann K. The role of the oral microbiome in obesity and

- metabolic disease: potential systemic implications and effects on taste perception. Nutr J 22: 28, 2023. doi:10.1186/s12937-023-00856-7.
- 97. Li H, Duncan C, Townend J, Killham K, Smith LM, Johnston P, Dykhuizen R, Kelly D, Golden M, Benjamin N, Leifert C. Nitratereducing bacteria on rat tongues. Appl Environ Microbiol 63: 924-930, 1997. doi:10.1128/aem.63.3.924-930.1997.
- Palmerini CA, Palombari R, Perito S, Arienti G. NO synthesis in human saliva. Free Radic Res 37: 29-31, 2003. doi:10.1080/ 1071576021000028398.
- Carlström M, Persson AE, Larsson E, Hezel M, Scheffer PG, Teerlink T, Weitzberg E, Lundberg JO. Dietary nitrate attenuates oxidative stress, prevents cardiac and renal injuries, and reduces blood pressure in salt-induced hypertension. Cardiovasc Res 89: 574-585, 2011. doi:10.1093/cvr/cvq366.
- Li X, Zhuge Z, Carvalho L, Braga VA, Lucena RB, Li S, Schiffer TA, Han H, Weitzberg E, Lundberg JO, Carlström M. Inorganic nitrate and nitrite ameliorate kidney fibrosis by restoring lipid metabolism via dual regulation of AMP-activated protein kinase and the AKT-PGC1α pathway. Redox Biol 51: 102266, 2022. doi:10.1016/j.redox. 2022 102266
- Gee LC, Massimo G, Lau C, Primus C, Fernandes D, Chen J, Rathod KS, Hamers AJ, Filomena F, Nuredini G, Ibrahim AS, Khambata RS, Gupta AK, Moon JC, Kapil V, Ahluwalia A. Inorganic nitrate attenuates cardiac dysfunction: roles for xanthine oxidoreductase and nitric oxide. Br J Pharmacol 179: 4757-4777, 2022. doi:10.1111/bph.15636.
- Bhaswant M, Brown L, McAinch AJ, Mathai ML. Beetroot and sodium nitrate ameliorate cardiometabolic changes in diet-induced obese hypertensive rats. Mol Nutr Food Res 61: 1700478, 2017. doi:10.1002/mnfr.201700478.
- Richter K, Konzack A, Pihlajaniemi T, Heljasvaara R, Kietzmann T. Redox-fibrosis: impact of TGFβ1 on ROS generators, mediators and functional consequences. Redox Biol 6: 344-352, 2015. doi:10.1016/ j.redox.2015.08.015
- 104. Liu ZY, Liu ZY, Lin LC, Song K, Tu B, Zhang Y, Yang JJ, Zhao JY, Tao H. Redox homeostasis in cardiac fibrosis: focus on metal ion metabolism. Redox Biol 71: 103109, 2024. doi:10.1016/j.redox.2024.103109.
- Schopfer FJ, Cipollina C, Freeman BA. Formation and signaling actions of electrophilic lipids. Chem Rev 111: 5997-6021, 2011. doi:10.1021/
- 106. Schopfer FJ, Khoo NK. Nitro-fatty acid logistics: formation, biodistribution, signaling, and pharmacology. Trends Endocrinol Metab 30: 505-519, 2019. doi:10.1016/j.tem.2019.04.009.
- Kansanen E, Bonacci G, Schopfer FJ, Kuosmanen SM, Tong KI, Leinonen H, Woodcock SR, Yamamoto M, Carlberg C, Ylä-Herttuala S, Freeman BA, Levonen AL. Electrophilic nitro-fatty acids activate NRF2 by a KEAP1 cysteine 151-independent mechanism. J Biol Chem 286: 14019-14027, 2011. doi:10.1074/jbc.M110.190710.
- 108. Palmer RM, Ferrige AG, Moncada S. Nitric oxide release accounts for the biological activity of endothelium-derived relaxing factor. Nature 327: 524-526, 1987. doi:10.1038/327524a0.
- Das S, Kumar KN. Nitric oxide: its identity and role in blood pressure control. Life Sci 57: 1547-1556, 1995. doi:10.1016/0024-3205(95) 02130-b.
- Siervo M, Lara J, Ogbonmwan I, Mathers JC. Inorganic nitrate and beetroot juice supplementation reduces blood pressure in adults: a systematic review and meta-analysis. J Nutr 143: 818-826, 2013. doi:10.3945/jn.112.170233.
- Bondonno CP, Croft KD, Hodgson JM. Dietary nitrate, nitric oxide, and cardiovascular health. Crit Rev Food Sci Nutr 56: 2036-2052, 2016. doi:10.1080/10408398.2013.811212.
- Ashworth A, Bescos R. Dietary nitrate and blood pressure: evolution of a new nutrient? Nutr Res Rev 30: 208-219, 2017. doi:10.1017/ S0954422417000063.
- Bourgoin F, Bachelard H, Badeau M, Melançon S, Pitre M, Larivière R, Nadeau A. Endothelial and vascular dysfunctions and insulin resistance in rats fed a high-fat, high-sucrose diet. Am J Physiol Heart Circ Physiol 295: H1044-H1055, 2008. doi:10.1152/ajpheart. 00516.2008.
- Heinonen I, Rinne P, Ruohonen ST, Ruohonen S, Ahotupa M, Savontaus E. The effects of equal caloric high fat and western diet

- on metabolic syndrome, oxidative stress and vascular endothelial function in mice. Acta Physiol (Oxf) 211: 515-527, 2014. doi:10.1111/ apha.12253
- Sanyal A, Poklepovic A, Moyneur E, Barghout V. Population-based risk factors and resource utilization for HCC: US perspective. Curr Med Res Opin 26: 2183-2191, 2010. doi:10.1185/03007995.2010.506375.
- Anstee QM, Reeves HL, Kotsiliti E, Govaere O, Heikenwalder M. From NASH to HCC: current concepts and future challenges. Nat Rev Gastroenterol Hepatol 16: 411-428, 2019. doi:10.1038/s41575-019-0145-7.
- Sawa T, Ohshima H. Nitrative DNA damage in inflammation and its possible role in carcinogenesis. Nitric Oxide 14: 91-100, 2006. doi:10.1016/j.niox.2005.06.005.
- Masarone M, Rosato V, Dallio M, Gravina AG, Aglitti A, Loguercio C, Federico A, Persico M. Role of oxidative stress in pathophysiology of nonalcoholic fatty liver disease. Oxid Med Cell Longev 2018: 9547613, 2018. doi:10.1155/2018/9547613.
- Bortolotti M, Polito L, Battelli MG, Bolognesi A. Xanthine oxidoreductase: one enzyme for multiple physiological tasks. Redox Biol 41: 101882, 2021. doi:10.1016/j.redox.2021.101882.
- 120. Haschek WM, Rousseaux CG, Wallig MA. Principles of toxicology. In: Fundamentals of Toxicologic Pathology, edited by Haschek W, Rousseaux C, Wallig M. London, UK: Academic Press, 2010, p. 1–8.
- Kozlov AV, Dietrich B, Nohl H. Various intracellular compartments cooperate in the release of nitric oxide from glycerol trinitrate in liver. Br J Pharmacol 139: 989-997, 2003. doi:10.1038/sj.bjp.0705323
- 122. Beddows CA, Shi F, Horton AL, Dalal S, Zhang P, Ling CC, Yong VW, Loh K, Cho E, Karagiannis C, Rose AJ, Montgomery MK, Gregorevic P, Watt MJ, Packer NH, Parker BL, Brown RM, Moh ES, Dodd GT. Pathogenic hypothalamic extracellular matrix promotes metabolic disease. Nature 633: 914-922, 2024. doi:10.1038/s41586-024-07922-v.
- Kang L, Ayala JE, Lee-Young RS, Zhang Z, James FD, Neufer PD, Pozzi A, Zutter MM, Wasserman DH. Diet-induced muscle insulin resistance is associated with extracellular matrix remodeling and interaction with integrin $\alpha 2\beta 1$ in mice. Diabetes 60: 416–426, 2011. doi:10.2337/db10-1116.
- 124. Chow CW, Kapus A, Romanek R, Grinstein S. NO₃-induced pH changes in mammalian cells. Evidence for an NO₃-H⁺ cotransporter. J Gen Physiol 110: 185-200, 1997. doi:10.1085/jgp.110.2.185.
- Khalifi S, Rahimipour A, Jeddi S, Ghanbari M, Kazerouni F, Ghasemi A. Dietary nitrate improves glucose tolerance and lipid profile in an animal model of hyperglycemia. Nitric Oxide 44: 24-30, 2015. doi:10.1016/j.niox.2014.11.011.
- 126. Huang PL. eNOS, metabolic syndrome and cardiovascular disease. Trends Endocrinol Metab 20: 295-302, 2009. doi:10.1016/j.tem. 2009.03.005.
- 127. Tousoulis D, Papageorgiou N, Androulakis E, Siasos G, Latsios G, Tentolouris K. Stefanadis C. Diabetes mellitus-associated vascular impairment: novel circulating biomarkers and therapeutic approaches. J Am Coll Cardiol 62: 667–676, 2013. doi:10.1016/j.jacc.2013.03.089.
- Matthews VB, Hollingshead R, Koch H, Croft KD, Ward NC. Longterm dietary nitrate supplementation does not prevent development of the metabolic syndrome in mice fed a high-fat diet. Int J Endocrinol 2018: 7969750, 2018. doi:10.1155/2018/7969750.
- Santamaria P. Nitrate in vegetables: toxicity, content, intake and EC regulation. J Sci Food Agric 86: 10-17, 2006. doi:10.1002/jsfa.2351.
- Carter P, Gray LJ, Troughton J, Khunti K, Davies MJ. Fruit and vegetable intake and incidence of type 2 diabetes mellitus: systematic review and meta-analysis. BMJ 341: c4229, 2010. doi:10.1136/bmj.c4229.
- Bondonno NP, Pokharel P, Bondonno CP, Erichsen DW, Zhong L, Schullehner J, Frederiksen K, Kyrø C, Hendriksen PF, Hodgson JM, Dalgaard F, Blekkenhorst LC, Raaschou-Nielsen O, Sigsgaard T, Dahm CC, Tjønneland A, Olsen A. Source-specific nitrate intake and all-cause mortality in the Danish Diet, Cancer, and Health Study. Eur J Epidemiol 39: 925-942, 2024. doi:10.1007/s10654-024-01133-5
- Yurekten O, Payne T, Tejera N, Amaladoss FX, Martin C, Williams M, O'Donovan C. MetaboLights: open data repository for metabolomics. Nucleic Acids Res 52: D640-D646, 2024. doi:10.1093/nar/ gkad1045.